Materials & Design 269 (2026) 116803

Contents lists available at ScienceDirect

Materials & Design

journal homepage: www.elsevier.com/locate/matdes

Upcycling recycled carbon fibres into hybrid limestone calcined clay cement (LC^3) composites for strengthening applications

Cesare Signorini [a,b,*], Jacopo Donnini [c,**], Anna Jose [a,b], Gianluca Chiappini [d], Marco Liebscher [a,b], Valeria Corinaldesi [c], Viktor Mechtcherine [a,b]

[a] Institute of Construction Materials, TU Dresden 01069 Dresden, Germany
[b] Cluster of Excellence CARE, TU Dresden and RWTH Aachen, Germany
[c] Department of Science and Engineering of Matter, Environment and Urban Planning (SIMAU), Università Politecnica delle Marche, Ancona, Italy
[d] Department of Theoretical and Applied Sciences, eCampus University, Novedrate 22060, Italy

ARTICLE INFO

Keywords:
Recycled carbon fibres
High-performance cement-based composites
Limestone calcined clay cement (LC^3)
Jacketing
Strengthening

ABSTRACT

A large share of structures worldwide cannot meet current design requirements due to updated anti-seismic guidelines, traffic growth, ageing, and severe climate change. High-Performance Fibre-Reinforced Cementitious Composites (HP-FRCC) represent an effective solution for structural strengthening; however, their widespread adoption is made less attractive by their high clinker content and reliance on virgin reinforcing fibres.

This study investigates the development of sustainable HP-FRCCs based on limestone calcined clay cement (LC^3) incorporating recycled carbon fibres (rCFs) recovered from end-of-life sources and brass-coated steel fibres (BSFs). Two commercially available rCFs were first characterised to identify the most suitable reinforcement before developing hybrid LC^3-based composites. The incorporation of rCFs increased compressive strength by up to 25% and flexural strength by more than 30% through microstructural refinement, while BSFs governed post-cracking behaviour and energy absorption. Hybridisation enabled the replacement of one third of the steel fibre content while maintaining confinement performance comparable to that of reference steel-fibre systems. Concrete cylinders strengthened with LC^3-HP-FRCC jackets exhibited compressive strength increases of up to 107% compared with unconfined specimens, together with significantly improved damage tolerance. The results demonstrate that combining rCFs with BSFs and LC^3 binders provides sustainable high-performance cementitious composites for structural retrofitting.

1. Introduction

High-performance cement-based composites (HPCCs) are an attractive technology that has recently been developed and investigated for a wide range of civil engineering applications, including large-span infrastructure, military and strategic buildings, and retaining systems. HPCCs are characterised by their outstanding compressive strength of over 80 MPa, which is due to their very low water-to-cement (w/c) ratio and extremely fine inert particles. This results in mixtures with a dense texture, which also improves durability by limiting chloride penetration [1,2]. Exceptional strength is guaranteed by the considerable amount of binder in the mix design — namely, ordinary Portland cement (OPC) combined with micro- and nano-sized pozzolanic materials. The addition of short, dispersed fibres can further enhance the mechanical response and the damage tolerance of HPCC [3,4], thereby expanding its range of applications to include design scenarios involving highly dynamic loading conditions [5–8]. More specifically, HPCCs comprise a significantly reduced dosage of coarse aggregates, with the dosage being eliminated in the so-called ultra-HPCCs (UHPCCs), in comparison to normal concrete (NC). In addition, HPCCs and UHPCCs contain approximately two and four times more cement, respectively, than NC [9]. The environmental impact of producing large quantities of OPC and quarrying fine quartz sand tends to be a limiting factor for HPCCs, restricting their use to niche applications such as the structural retrofitting of concrete piers and beams, where thin layers of material are required [10,11]. Traditionally, the reduction of clinker content has relied on sup plementary cementitious materials (SCMs), including fly ash (FA), ground granulated blast furnace slag (GGBS), silica fume (SF),

* Corresponding author at: Institute of Construction Materials, TU Dresden, 01069 Dresden, Germany.
** Corresponding author.
E-mail addresses: cesare.signorini@tu-dresden.de (C. Signorini), jacopo.donnini@staff.univpm.it (J. Donnini).

https://doi.org/10.1016/j.matdes.2026.116803
Received 15 May 2026; Received in revised form 25 July 2026; Accepted 15 August 2026
Available online 16 August 2026
0264-1275/

and natural pozzolans. While these materials have significantly contributed to lowering the environmental footprint of cement-based materials, the future availability of FA and GGBS is expected to decrease owing to the progressive decarbonisation of the energy and steel industries. Consequently, increasing attention has shifted towards alternative SCMs derived from natural resources. Among these, limestone calcined clay cement (LC^3) has emerged as one of the most promising low-carbon binder systems, due to its vast global availability, lack of reliance on industrial by-products, compatibility with existing cement manufacturing technology, and ability to achieve high clinker substitution. LC^3 binders with 50% clinker replacement have been reported to reduce CO_2 emissions by approximately 30–40% compared to OPC binders [12], while maintaining comparable or superior mechanical performance and durability [13–15]. Building on this idea, high-performance and pseudo-ductile composites have been conceptualised and developed for structural strengthening [16,17], with the proportions of the binders in the blend designed to achieve the target strength [18]. To further advance the circularity of HPCC, the possibility of embedding fibres retrieved from secondary sources has been widely explored, particularly recycled steel [19,20] and carbon fibres [21,22]. In a recent review, Abdolpour et al. [19] outlined the use of steel fibres obtained from recycled materials, such as scrap tyres and spent equilibrium catalysts from oil refineries. These materials demonstrate great potential for reducing costs and mitigating the environmental footprint of ultra-high-performance fibre reinforced concrete (UHPFRC). Patchen et al. [22] recently published an experimental study in which they attempted to incorporate recycled carbon fibres of different shapes (i.e. chopped fibres and platelets) obtained from aerospace applications into high-performance concrete formulations, reporting significant increases in tensile and compressive strength. In general, the extent of performance improvement depends heavily on the bond between the fibres and the matrix, which is generally poor for carbon fibres [23–25], leading to pronounced pull-out failure under loading and poor crack bridging capacity. The most common source of recycled carbon fibres is end-of-life fabric-reinforced polymer (FRP) composites that were originally used as components in the automotive or aerospace industries. Global production of carbon-fibre reinforced composites has increased rapidly over the last two decades, resulting in an estimated 62,000 tonnes of end-of-life carbon fibre-reinforced polymer (CFRP) waste currently generated every year. This figure is expected to increase dramatically as aircraft, wind turbine blades and automotive components progressively reach the end of their service life, with annual waste generation projected to exceed 150,000 tonnes by 2050. Consequently, identifying high-value applications for recycled carbon fibres has become an important challenge for the circular economy [26]. To successfully upcycle end-of-life FRP, the fibres require processing to remove the original sizing and impregnation. The main treatment methods are based on three principles: (i) mechanical recycling, which involves shredding, grinding and sieving; (ii) chemical processing; and (iii) thermal processing. Of these techniques, thermal recycling, i.e. pyrolysis, is the most frequently used due to its industrial scalability. Pyrolysis generally removes the impregnating resin as well as any pre-existing sizing on the carbon fibres. This process involves heating the FRP elements to 750°C in an inert atmosphere, which degrades any residual polymeric phase while retaining satisfactory levels of mechanical properties compared to mechanically recovered carbon fibres. The extent to which this occurs depends on the parameters of the recovery process [27,28]. The use of steel or carbon fibres to reinforce cementitious composites generally aims to improve the stiffness and tensile/flexural properties of HPFRC and UHPFRC for specific applications, such as jacketing and confining reinforced concrete columns or piers subjected to a combination of normal and bending loads. The aim is to restore their structural robustness and safety by demonstrating remarkable improvements in their flexural and shear capacity, as well as their ductility [29–33], empowered by the bridging action of the fibres [34]. Most studies on the confinement of concrete elements have focused on HPFRC matrices reinforced with short steel fibres [35–37], whereas only a limited number of studies have investigated the strengthening of masonry walls [38] or columns [39] using HPFRC.

Although these classes of strengthening materials show clear potential, the confining effect of high-performance matrices based on blended binders incorporating hybrid fibre reinforcement in retrofit applications has yet to be fully investigated, particularly when using limestone calcined clay cement (LC^3), owing to its growing importance as a low-carbon alternative to ordinary Portland cement. Adopting a practical, application-oriented approach, this paper thoroughly characterises two chopped carbon fibres retrieved from post-industrial prepreg textile scraps and post-consumer/end-of-life CFRP laminates, respectively. Following the preliminary characterisation of the two rCF types, the rCF exhibiting the most consistent and reliable physical and mechanical properties was selected for further investigation. High-performance fibre reinforced cementitious composites (HP-FRCC) formulations were then developed using rCFs and commercially available brass-coated steel fibres (BSFs), either separately or in combination, embedded in an LC^3-based fine-grained concrete matrix with 50% OPC replacement. The fresh and hardened properties of the selected formulations were screened using spread flow measurements, compression, bending and tensile tests. The application of LC^3-based HP-FRCC in jacketing laboratory-scale concrete cylinders is also presented as a pilot case study. Design-oriented analytical models from the literature, as well as those proposed by the Italian National Research Council (CNR–DT 215) and by the American Concrete Institute (ACI 549.6R-20) guidelines, have been applied in this study to evaluate their predictive capability for the confinement of concrete cylinders with LC^3-HP-FRCC. While these analytical models govern the design of confinement with textile-reinforced mortar applications, there is adequate agreement with the experimental findings presented here.

2. Materials and methods

2.1. Raw materials

2.1.1. Short fibres

This study investigates and compares two varieties of recycled carbon fibres (rCFs) to chopped virgin carbon fibres (vCFs) as a benchmark (Sigrafil®-C-C5-4.0/240-E100). Both sorts of rCF (R-rCF, supplied by Rymyc Srl, Italy, and M−rCF, carboNXT, supplied by Marubeni International (Europe) GmbH, Germany) were pyrolysed by the manufacturer to remove the original polymeric impregnation and sizing. The R-rCFs ("R" standing for "*Rymyc*") were retrieved from post-industrial scraps of pre-preg textiles that were no longer usable in manufacturing production lines due to shelf-life limitations, while M−rCFs ("M" standing for "*Marubeni*") were derived from batches of disposed end-of-life CFRP laminates typically used in automotive and aerospace applications. No additional surface treatment was applied after the industrial recycling process carried out by the manufacturers.

In addition, straight high-carbon brass-plated steel fibres (BSF) were supplied by La Matassina (Isola Vicentina, Italy), measuring 13 mm in length and 200 μm in diameter. These fibres are commonly adopted in high- and ultra-high-performance concrete mixtures and are characterised by a brass coating that mitigates their vulnerability to corrosion.

Fig. 1 shows the appearance of the BSFs and rCFs, with a particular emphasis on their significantly different diameters, while Table 1 reports the properties of all the fibres at hand as declared by the manufacturers. The nominal diameter of the carbon fibres (CFs) is approximately 7 μm, whereas the experimentally measured lengths of the rCFs was found to range from 10 to 30 mm, deviating from the nominal value declared by the manufacturers. Such variability is inherent to recycled carbon fibres due to the recycling and processing methods. As shown in previous studies, this specific BSF grade exhibits a consistent, cylindrical shape characterised by smooth surfaces [40].

(a) Brass-plated Steel fibres (BSF) (b) Recycled Carbon fibres (R-rCF) (c) Recycled Carbon fibres (M-rCF) (d) Difference in diameter

Fig. 1. Appearance of the fibres investigated in the current study.

Table 1
Physical and mechanical properties of rCF, vCF and BSF, as declared by the manufacturers.

Property	Unit	R-rCF	M−rCF	vCF	BSF
Material	–	Carbon	Carbon	Carbon	Steel
Density	[g/cm^3]	1.80	1.80	1.80	7.87
Length	[mm]	20	12	12	13
Diameter	[µm]	7	7	7	200
Tensile strength	[MPa]	n.a.	3500 (min.)	4000	3100
Tensile modulus	[GPa]	n.a.	230 (min.)	240	n.a.
Sizing/coating	–	No	No	No	Brass

2.1.2. Limestone calcined clay cement (LC^3) fine-grained matrix

The embedding matrix consists of a blended ternary binder, made from OPC, limestone, and calcined clay, with optimised rheology for automated construction technologies [41–43]. The binder system consists of (i) OPC type I, having a compressive strength of 52.5 MPa and high resistance to sulphates, (ii) calcined clay obtained from a low-grade, widely available raw source with an amorphous content of 55% after calcination [16], and (iii) limestone. The clinker factor of the proposed mix is 0.5, and two parts of calcined clay are mixed with one part of limestone by weight. The particle size distribution, density, chemical composition, and mineralogical composition of OPC, calcined clay, and limestone were previously investigated and reported in detail in our earlier studies [18,42]. The dosages listed in Table 2 derive from prior research on high-performance LC^3 binders for structural protective composites. This formulation leverages the concept that high-performance LC^3 matrices exhibit optimal bond with high-performance fibres, as demonstrated in the scale-linking investigation by Ahmed et al. [44]. This fine-grained concrete formulation has been developed as a matrix for strain-hardening cement-based composites (SHCC), which exhibited enhanced toughness and impact resistance [6].

Table 2
Composition of the LC^3 fine-grained matrix.

Constituent	Role	Sort / Manufacturer	Dosage [g/dm^3]
OPC	Binder	CEM I 52.5R-SR3 (na), Holcim, DE	599
Calcined clay		Liapor, DE	379
Limestone powder		Saxodol 90 LE, sh-minerals, DE	190
Calcium sulphate		Dihydrate (gypsum), Grüssing, DE	30
Quartz sand	Inert aggregates	BCS 413, Strobel, DE	536
Superplasticizer	Admixtures	Glenium ACE 460, BASF, DE	11
Viscosity stabiliser		UW Compound – 100®, Sika, CH	2
Water (tap)			359

2.2. Specimen manufacturing and test protocols

2.2.1. Mixing procedure

The fibre dispersion quality and the macroscopic homogeneity of the composite systems were carefully ensured by optimising the mixing protocol through an extensive preliminary campaign. Specific parameters, including fibre stirring, mixing time, shear energy, were systematically refined to prevent agglomeration and bundling. Due to the strong tendency of CFs to bundle, a wet-mix approach was adopted to manufacture prismatic specimens. This method enhances rCF distribution within the cementitious matrix, as the fibres chemically interact with the superplasticisers in the wet mix. As illustrated in Fig. 2, initially, the rCFs were placed in a plastic bucket equipped with a small aperture for a compressed-air gun, which was used to stir and thoroughly disaggregate the fibres. The rCFs were then gradually introduced into the water, followed by the addition and thorough mixing of the water-reducing agent. This aqueous mixture was slowly added to the dry constituents — which had been pre-mixed for 4 min in a Hobart mixer — and blended for 2 min at 107 rpm. The fresh-state mixtures exhibited high batch-to-batch consistency in terms of workability and flowability. No visual evidence of fibre nesting or segregation was observed during either the flow tests or the subsequent casting operations within the thin moulds. Following this mixing protocol, the characterisation of the fresh properties was performed and specimens for mechanical tests were cast, as detailed in the following sections.

2.2.2. Preliminary characterisation of the rCF

2.2.2.1. Morphology and diameter. The surface morphology of the fibres and the actual distribution of fibre diameters were measured directly using a Quanta 250 (The Netherlands) scanning electron microscope (SEM) equipped with a field emission gun (FEG).

2.2.2.2. Physical and mechanical properties. To assess the thermal stability of rCFs, thermogravimetric analyses (TGA) are conducted on rCFs using a STA 409 DC thermal analyser (Netzsch, Germany) and compared with vCFs that have not undergone pyrolysis. Samples of each type of carbon fibre were subjected to a thermal ramp of 10 °C/min up to 1000 °C in an oxygen environment with a flow rate of 60 mL/min.

The tensile strength of the single fibres is measured by using a Zwick Roell 1445 universal testing machine equipped with a load cell with a capacity of 10 N and a test speed set to 0.01 mm/s, following the protocol established by Ranjbarian and Mechtcherine [45].

Each specimen is an individual fibre, the ends of which were carefully glued to a rectangular paper frame. The free length of the fibre (i.e. the open span of the paper frame) is 20 mm. The paper frame was then clamped to the testing machine using special grips, which were then firmly tightened with screws. The lateral parts of the paper were cut off before the tests were carried out [46]. The schematic representation of the single fibre tensile test setup is provided in Fig. 3. Due to the delicate

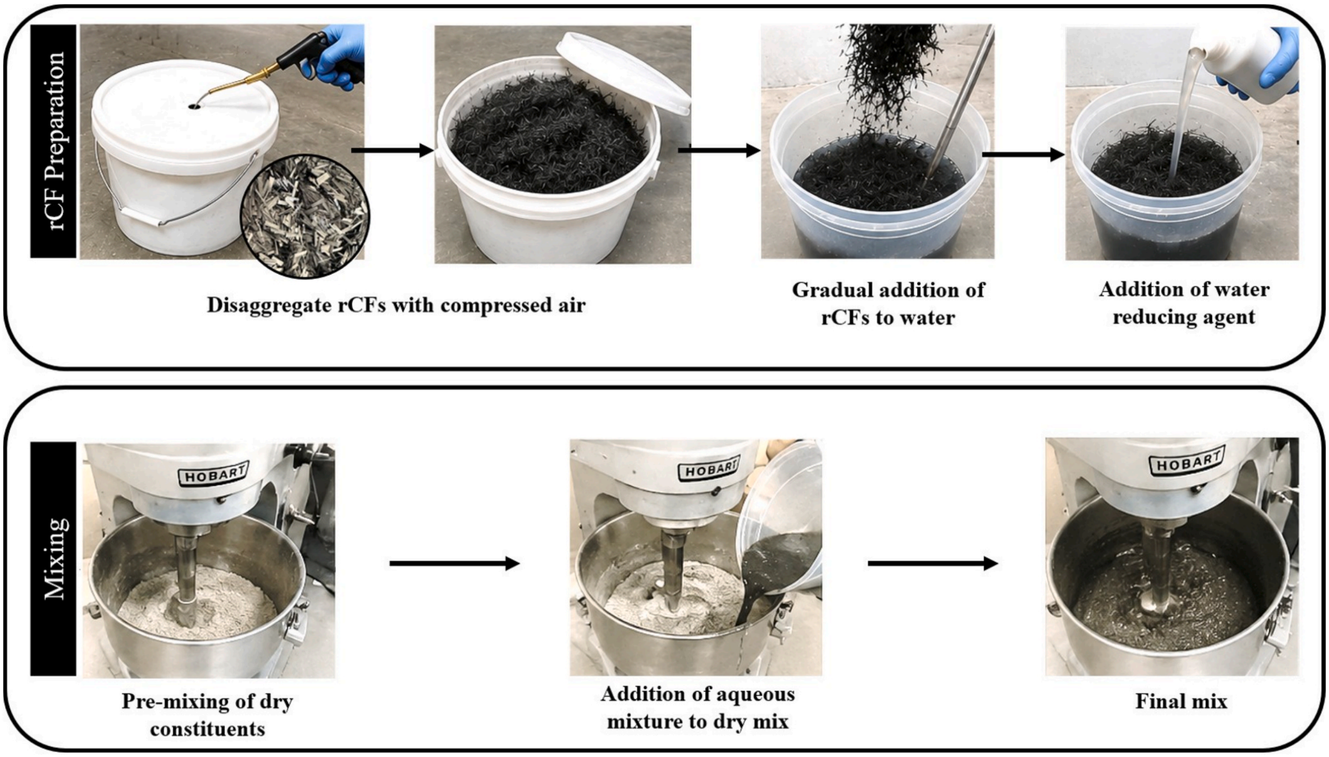

Fig. 2. Schematic illustration of the rCF-reinforced mortar mixing procedure.

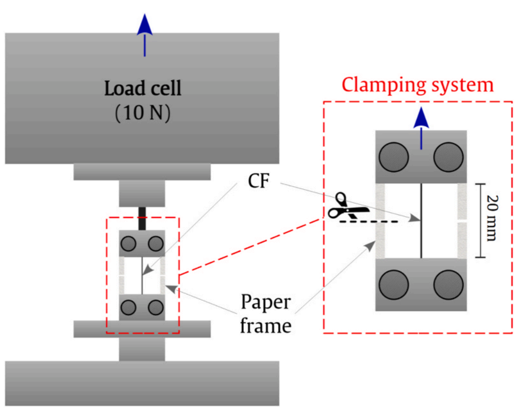

Fig. 3. Testing set-up for single-fibre tensile tests (adapted from Li et al. [47]).

handling of single carbon fibres and their extreme brittleness, at least 15 samples were manufactured, and the results were obtained from at least five successful tests. The aim of single-fibre tensile tests is to determine the possible reduction in the mechanical performance of rCF compared to their virgin counterparts due to the recycling process, particularly the thermal treatment.

2.2.3. Characterisation of the HP-FRCC

To determine the effect of CFs on the workability of the HP-FRCCs in their fresh state, Hägermann table flow analyses were conducted in accordance with EN 12350–5. Briefly, a sample of the fresh composite was placed in a hollow conical mould arranged in the centre of a glass table. The surface of the sample was levelled using a scraper, after which the mould is carefully removed. Once the composite has spread, 15 S are applied to the glass flow table. The spread diameter is measured in two perpendicular directions, both before and after the strokes, and the mean values are referred to as BS and AS, respectively. In addition, the air content of the fresh mixes was assessed in conformity with the protocol recommended in the EN 12350–7 standard, using a one-litre mould filled with three layers of the mix, which were then compacted and levelled. Any entrapped air was removed prior to measurement. The fresh mixture was cast in a standard mould to produce prismatic beams with a cross-section of 40 × 40 mm^2 and a length of 160 mm, which were then used for three-point bending tests. After curing inside the moulds for 24 h, the specimens were demoulded, lightly sprinkled with water, sealed in plastic bags to maintain approximately 100% relative humidity, and stored in a climatic chamber at 22°C for a further 27 days. Bending tests were then performed using a universal testing machine set to a stroke-controlled regime of 0.05 mm/s. The two broken halves of the beams were subsequently tested under compression using a 40 × 40 mm^2 imprint at a load-controlled setup of 2.5 kN/s to evaluate the strength of the HP-FRCCs. Three volumetric dosages of rCFs (i.e., 0.5%, 1.0%, and 1.5%) were investigated to ascertain whether optimal performance could be attained. The testing matrix of the HP-FRCC is given in Table 3. Combinations that lead to poor workability standards and are deemed unsuitable for pouring are disregarded, particularly as rCF content increases.

2.2.4. Concrete jacketing

2.2.4.1. HP-FRCC formulations for concrete jacketing: selection criteria and tensile testing. Based on the results of the mechanical characterisation screening tests carried out on the LC^3-HP-FRCC matrices, three of them have been selected for the confinement of small-scale demonstrative concrete cylinders. The choice was made by taking into consideration both the mechanical properties and workability of the matrices in their fresh state (with a spread diameter of at least 200 mm). This ensures that they can be cast as a 30 mm thick strengthening confining layer by pouring the fresh mixes. The three selected HP-FRCCs were those including only one type of fibre, i.e. (i) 1% M−rCF and (ii) 1.5% BSF; as well as (iii) a hybrid solution that included both 0.5% M−rCF and 1% BSF (the fibre dosages are given as volume fractions).

Table 3
Test matrix for the characterisation of the fresh and hardened properties of the HP-FRCCs.

rCF dosage[% vol.]	BSF dosage[% vol.]	Tests
0	0	Compressive / Bending
0	0.5	Flow / Compressive / Bending
0	1.0	Flow / Compressive / Bending
0	1.5	Flow / Compressive / Bending / Tensile* / Cylinder jacketing*
0	2.0	Flow / Compressive / Bending
0.5	0	Compressive / Bending
0.5	0.5	Flow / Compressive / Bending
0.5	1.0	Flow / Compressive / Bending / Tensile* / Cylinder jacketing*
1.0	0	Compressive / Bending / Tensile* / Cylinder jacketing*
1.0	0.5	Flow / Compressive / Bending
1.0	1.0	Flow / Compressive / Bending
1.5	0	Compressive / Bending

* = Tensile tests and cylinder jacketing are conducted with M−rCF only as case studies (see §2.2.4).

The volume of rCFs was restricted to 1% (or 0.5% for the case of hybrid reinforcement) to ensure adequate flowability of the matrix. In addition to the compression and bending tests presented in Section 2.2.3, uniaxial tensile tests were also carried out on dog-bone shaped HP-FRCC specimens for these three selected formulations. The specimens were cast in wooden formworks, demoulded after one day, sealed in plastic bags, and cured at 20 ± 2 °C for 60 days prior to testing.

The geometry and dimensions of the specimens for tensile testing are reported in Fig. 4a. The gripping system (Fig. 4b), consisting of four metal cylinders at the ends of the specimen, was designed to minimise the effects of misalignment along the longitudinal direction, as well as bending stresses and eccentricity, during the test. Uniaxial tensile tests were performed in displacement control on a Zwick Z050 universal testing machine with a maximum load capacity of 50 kN, at a loading rate of 0.5 mm/min. Displacements and strains within the gauge section of HP-FRCC specimens during tensile tests were measured using a Digital Image Correlation (DIC) acquisition system. The stress–strain curves and strain maps were evaluated in a rectangular region of interest (ROI) corresponding to the front face of the specimen over a length of 140 mm. The image sequence was analysed using a digital image correlation algorithm in the commercial software MatchID, which employs a subset-based DIC formulation. The subset size was set to 21 × 21 pixels, with a step size of 5 pixels.

2.2.4.2. Characterisation of HP-FRCC-jacketed concrete cylinders. The potential of the developed HP-FRCCs as an external strengthening system for concrete structures was preliminarily evaluated through a pilot-scale application. To simulate the retrofitting of existing low-strength reinforced concrete elements, eight concrete cylinders (135 mm in diameter and 400 mm in height) were cast using a low-performance concrete. The substrate concrete was produced using OPC CEM II/B 32.5R, with a water-to-cement ratio (w/c) of 0.62, 330 kg/m^3 of calcareous sand (0 – 4 mm), and 985 kg/m^3 of coarse calcareous aggregate with a maximum particle size of 20 mm. The average compressive strength of the substrate concrete, determined on standard cubes (100 × 100 × 100 mm^3) in accordance with EN 12390–3 after 90 days of curing at a temperature of 20 ± 2 °C, was 17.8 MPa (CoV = 2%).

Concrete cylinders were cast using plastic formworks and demoulded after 48 h. They were then cured under laboratory conditions for 28 days before being strengthened. Six of the cylinders were confined with a layer of the three different selected HP-FRCCs (two repetitions for each HP-FRCC type), using a cylindrical plastic formwork with an internal diameter of 195 mm to manufacture a 30 mm thick external jacket (see Fig. 5a). Before casting the HP-FRCC layer, the external surface of the concrete cylinders was sanded, cleaned with compressed air and wetted with water. The strengthened cylinders were then cured for 60 days at a temperature of 20 ± 2 °C before undergoing compression testing. Unreinforced (reference) concrete cylinders were cured under the same conditions for a total of 90 days prior to testing.

Uniaxial compression tests were performed using a Galdabini compression machine with a maximum capacity of 1500 kN, in displacement control at a rate of 0.5 mm/min. Particular attention was paid to the application of the axial load by using two cylindrical steel plates of the same diameter as the internal concrete cylinder to ensure that the external reinforcement layer was not loaded directly (see Fig. 5a,b). The compression test results are reported as stress–strain curves in Fig. 16. The axial compressive stress is calculated by dividing the compressive load by the cross-sectional area of the unreinforced concrete cylinder (diameter of 135 mm), while the peak stress, reported

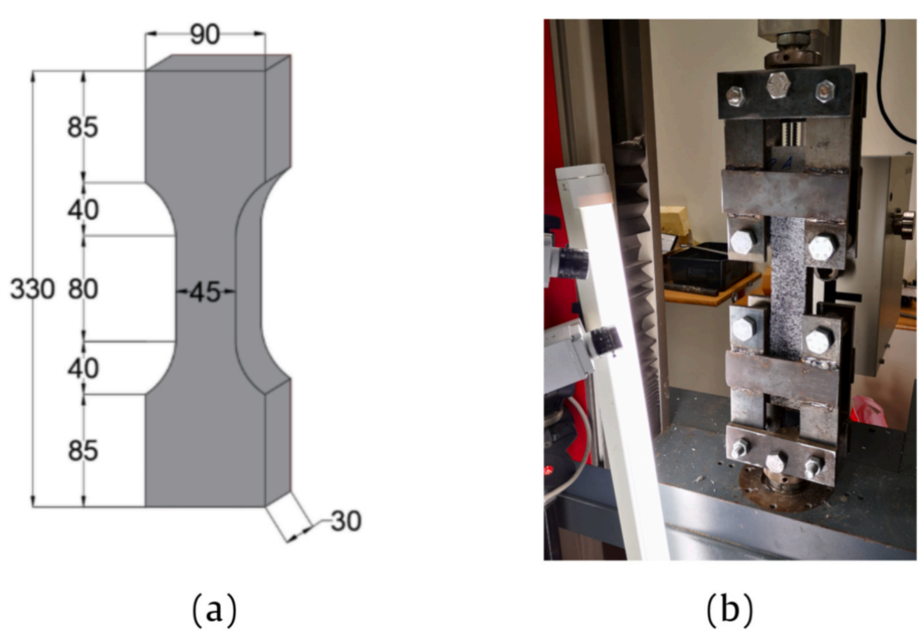

Fig. 4. Uniaxial tensile test on LC^3-HP-FRCC dog-bone shaped specimens: (a) specimen geometry and (b) tensile test setup with DIC acquisition system.

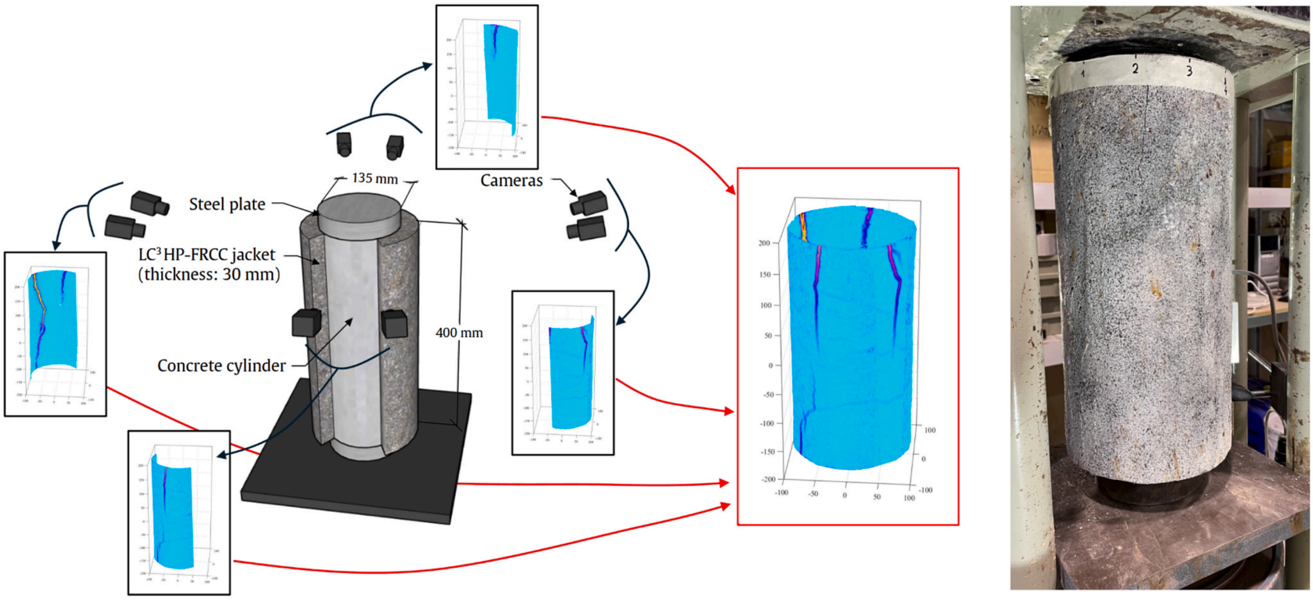

(a) Specimen geometry and optical monitoring through DIC (b) Test setup

Fig. 5. Compression test on confined concrete cylinders.

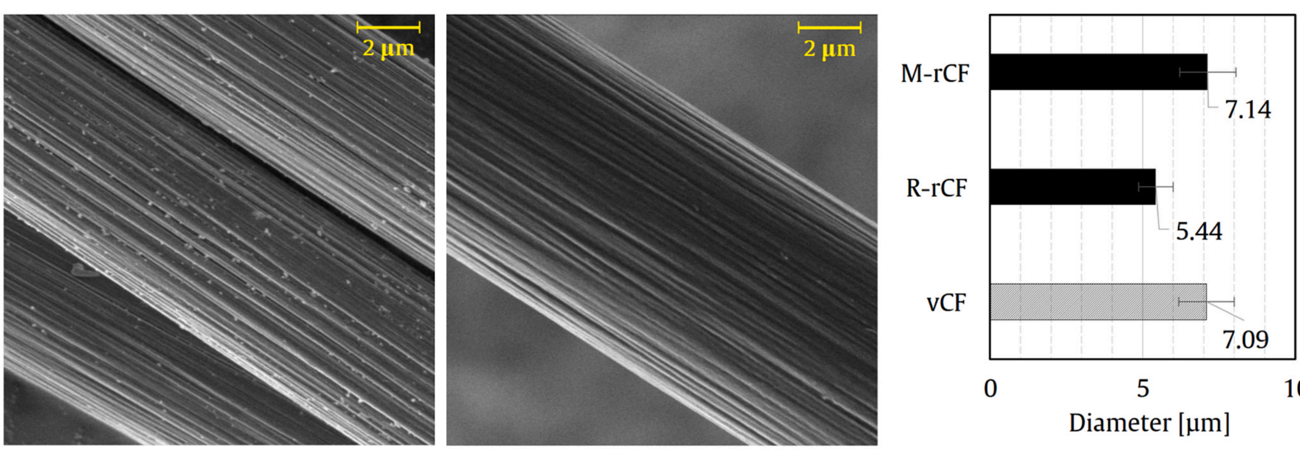

(a) R-rCF (b) M-rCF (c) Diameter of carbon fibres

Fig. 6. Visualisation of the rCF surface morphology from SEM and average diameters in comparison with vCFs as investigated by Li et al. [47]. Picture credit: Dr Thomas Köberle, TUD.

in Table 5, is the maximum load reached during the test, normalised by the same area. The approach of considering only the area of the reinforced element, without accounting for the contribution of the reinforcement area, has been adopted in several studies reported in the literature [35,36,39]. Stress–strain curves were obtained by plotting both the vertical and horizontal strains measured on the external surface of the specimens. The term *'external surface'* refers to the lateral surface of the specimens, i.e. the concrete cylinder for the reference specimens and the HP-FRCC jacket for the reinforced ones.

The external cylindrical surface of the specimen was monitored using a DIC system composed of eight cameras arranged in four stereo pairs. Each stereo pair allowed the reconstruction of approximately 110–120° of the specimen surface. By combining the four reconstructed sectors, the full cylindrical surface was obtained, as shown in Fig. 5a. The DIC analysis was carried out using the commercial software MatchID. The displacement fields obtained from each stereo pair were subsequently exported and processed in MATLAB, where the four datasets were merged to reconstruct the full-field displacement distribution over the entire cylindrical surface. Starting from the reconstructed geometry and displacement field, the strain field was computed by adopting a cylindrical coordinate system. This transformation enabled the evaluation of the vertical axial strain (ε_v), aligned with the loading direction, and the circumferential strain (ε_h) , associated with the hoop direction of the cylinder. These strain components were used to derive the curves reported in Fig. 16. Finally, the equivalent strain maps obtained over the entire reconstructed surface were used to monitor crack initiation and propagation during the test, enabling the assessment of the evolution of the cracking pattern (Fig. 17).

3. Results and discussion

3.1. Screening and selection of the rCFs

This section presents the characterisation results of the two types of recycled carbon fibre, namely R-rCF and M−rCF, to identify the most suitable for use in hybrid LC^3-HP-FRCC. Fig. 6 shows the appearance of the surfaces of the two types of rCF, together with their average diameter, which was measured using SEM investigations, with an average of more than 20 measurements taken. The results were then compared with those for virgin carbon fibres (vCF), as measured by Li et al. [47].

The two varieties of rCFs differ slightly in surface appearance. In both cases, pronounced longitudinal grooves can be observed that appear to be deeper than those of virgin carbon fibres [47], confirming the evidence of other independent studies on the topic (see Belli et al. [48]). Such imperfections developing on the surface of rCFs can obviously have an adverse effect on tensile properties, but they can also entail beneficial effects by promoting mechanical interlocking with the surrounding matrix. In contrast to the observations of Guo et al. [49] regarding rCFs produced by pyrolysis (i.e. in an argon environment), no residues of pyrolytic carbon originating from the decomposition of sizing agents or impregnation of the pristine textile were found to be deposited on the surface of the analysed rCFs. However, some contamination is visible, particularly for R-rCF, probably due to environmental impurities. Conversely, a significant difference can be noted in the average diameters measured by SEM. While M−rCFs have a similar diameter to virgin carbon fibres, R-rCFs have a diameter that is 24% smaller than vCFs. This cannot be attributed solely to the removal of fibre sizing (approximately 3–5%) [50,51] and may strongly influence their tensile behaviour.

Fig. 7 illustrates the tensile properties of the two types of rCF in terms of stress–strain curves (inlet *a*), average tensile strength and elastic modulus (inlets *b* and *c*, respectively). As would be anticipated from the defects observed on the fibre surface, rCFs show a notable decline in tensile strength after the recycling process when compared with vCF. The reduction in strength was 26% and 36% for M−rCF and R-rCF, respectively, which turned out to be more severe than in similar studies. For instance, Jiang and Pickering [52] found reductions ranging from 5% to 16%. However, this result can be explained by the fact that our study focuses on recycled fibres taken from actual industrial batches of end-of-life textiles. The origin and properties of these fibres are characterised by pronounced scatter and differ from those of the virgin counterpart.

Notably, M−rCFs retain the original stiffness of carbon fibres, with a modulus 50% higher than that of R-rCFs, as demonstrated by the slope of the pure elastic curves of the individual filaments (Fig. 7a). The oxidation behaviour of the fibres is presented in Fig. 8, in terms of mass loss as a function of temperature. The presence of the original sizing in vCF results in slightly higher mass loss at earlier stages compared to recycled counterparts where the sizing has been thermally removed before. Indeed, for rCFs no significant degradation is detected before 550 °C. Consequently, a 10% mass loss was measured for vCF at around 598 °C. The same mass loss threshold was observed for rCFs at higher temperatures, i.e. 631 °C (M−rCF) and 626 °C (R-rCF), at which point the oxidation process began and led the fibres started to lose their integrity. Nevertheless, all fibres underwent full oxidation at around 800°C. Interestingly, M−rCF exhibited a residual mass of approximately 4% above 800°C, which can be attributed to the presence of metallic traces that could have been introduced in the manufacturing process or as catalysts, as well as impurities [53]. Once again, a slight improvement in the thermal properties of the recycled fibres was observed compared to the virgin fibres. This is likely linked to the pyrolysis process, which is believed to enrich the fibres with more stable graphite crystals following the thermal transformation of the amorphous portions [54]. To select the most stable rCF type for incorporation into cementitious composites, it is worth noting that M−rCFs undergo most of their oxidation within a narrower temperature range, as also indicated by the sharpest peaks on the differential heat curve. This key indicator reflects the highest oxidation temperature and suggests the utmost homogeneity and the presence of fewer impurities in its composition, making M−rCF more thermally stable than R-rCF [55]. Regarding the mechanical performance of rCF composites, Fig. 9 and Fig. 10 respectively depict the variation in the flexural and compressive strength with increasing rCF dosage.

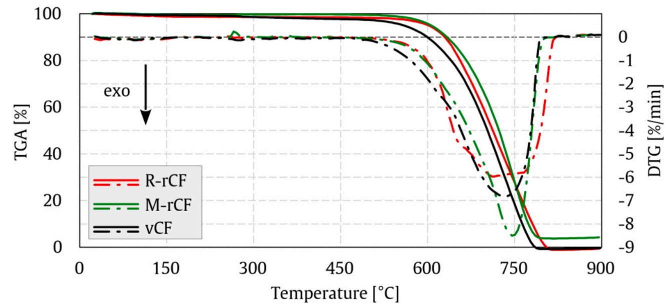

Fig. 8. TGA profiles for both kinds of rCF in oxygen atmosphere (vCF added as a term of comparison).

The volume fractions range from 0% (plain fine-grained concrete matrix) to 1.5%, since higher rCF dosages have been shown in Donnini et al. [56] to impair the fresh properties of the composite, rendering it unsuitable for casting in thin moulds or for special applications [57]. The individual stress–strain curves are not presented in this paper as the material behaviour is found to be the same for all composites, i.e. pseudo-elastic up to brittle failure. As a general observation, the two types of fibre induce a similar improvement in the mechanical properties of the high-performance, fine-grained concrete matrix. Although the difference is not statistically significant in all cases, M−rCF addition results in a slight improvement in bending strength, whereas a reverse trend is observed for compressive strength. The reasons for this

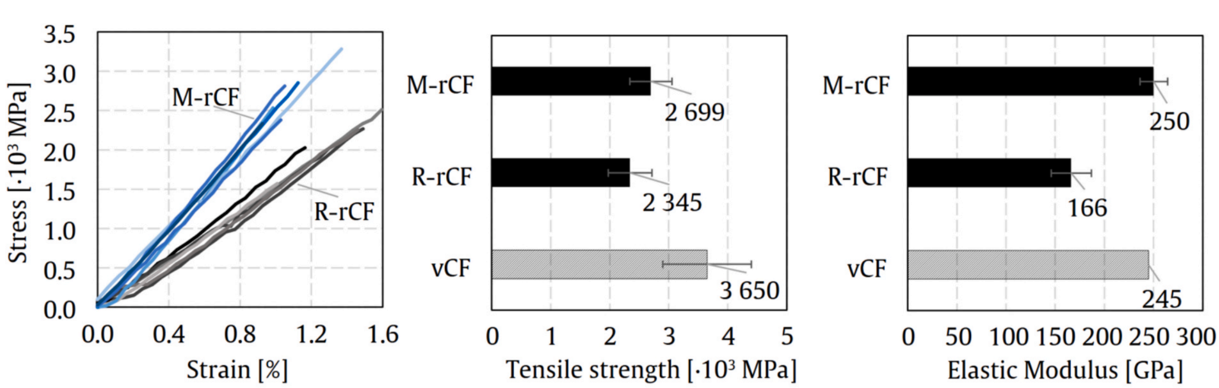

(a) Strength curves for rCF
(b) CF tensile strength
(c) CF modulus of elasticity

Fig. 7. Tensile test results in terms of stress–strain curves for rCF, and bar-charts for CF strength and modulus, compared with vCF [47].

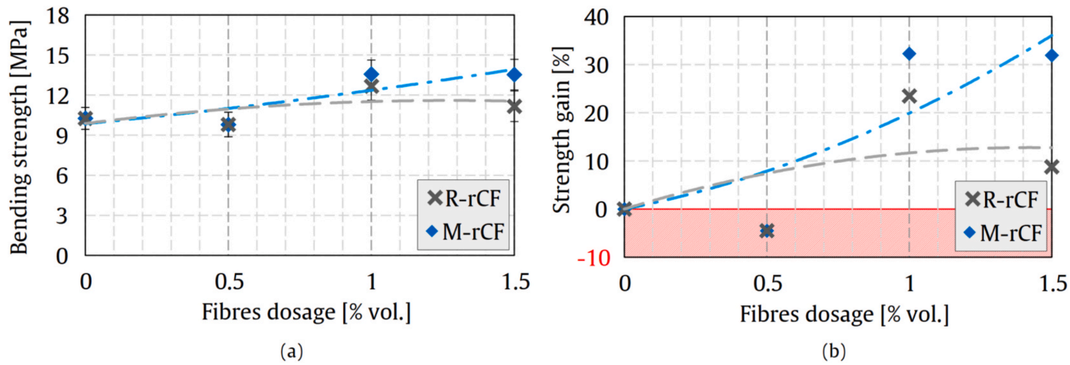

Fig. 9. Bending strength variation of HP-FRCC including rCF in increasing dosages.

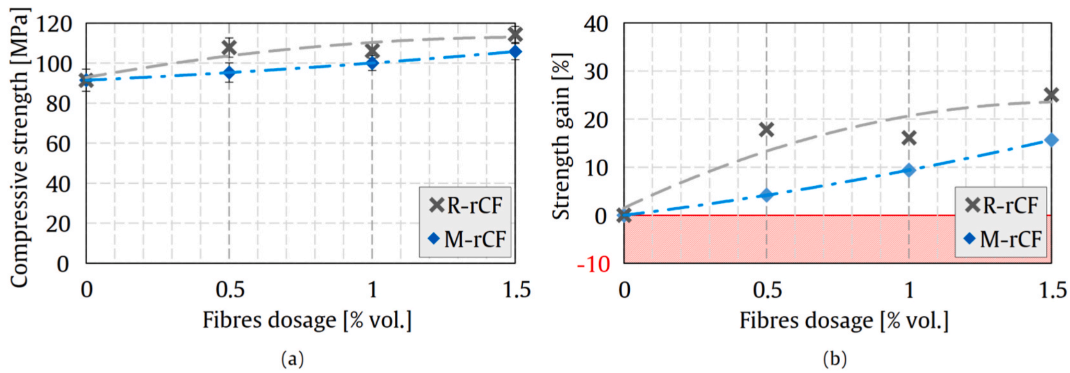

Fig. 10. Compressive strength variation of HP-FRCC including rCF in increasing dosages.

discrepancy require further investigation, which is beyond the scope of this work. However, it can be presumed that the larger diameter of the M−rCFs (31% larger than that of R-rCFs, on average) reduces the number of broken fibres during mixing and casting, thereby slightly improving the bridging action of the fibres and delaying bending failure, albeit marginally. The improvement in strength, which is mainly promoted by good fibre dispersion in the matrix, is attributed to the filler effect of the broken carbon fibres within the matrix. Indeed, previous studies recognise that, even at limited volume fractions, carbon fibres are pivotal in reducing porosity by acting as nucleation sites; this accelerates hydration reactions, delays microcrack onset and clustering, and provides microscale crack bridging [58]. Within the domain of ultra-high-performance concrete, Meng and Khayat demonstrated an approximate 4% increase in compressive strength through the incorporation of 0.3% carbon nanofibres [59]. Previous studies also confirm that this effect is more pronounced in more porous (lower strength) concrete matrices due to their greater porosity. Nevertheless, improvements in compressive strength of between 10% and 25% and in bending strength of more than 30% are achieved in high-performance fine-grained concrete due to the combined effect of fibre bridging and the filler effect [60].

Based on the physical, mechanical, and composite properties of both rCF types, experimental tests were performed on HP-FRCCs using M−rCFs. While achieving similar reinforcing effects (see Fig. 9 and Fig. 10), M−rCF exhibit significantly higher dimensional consistency, superior mechanical performance, and enhanced thermal stability compared to R-rCFs (Fig. 7 and Fig. 8). Furthermore, although recovering post-consumer carbon fibres (M−rCFs) involves more complex processing than post-industrial waste (R-rCFs), this stream is scientifically justified to achieve full lifecycle circularity and mitigate landfilling. Looking ahead, manufacturing efficiency will decrease post-industrial waste availability by reducing scraps. Conversely, post-consumer M−rCF address the massive, growing volume of end-of-life composites, aligning with long-term industrial sustainability and legislative mandates.

In the following sections, the threshold volume fraction for M−rCF is set at 1% to ensure the mix is workable enough for the intended jacketing application. Despite this upper limit being common in the literature [61,62], using M−rCF introduces higher amounts of recycled material into the system than in previous studies where volume fractions of up to 0.3% could be incorporated into FRC blends hybridised with steel fibres [63].

3.2. *Characterisation of HP-FRCC systems*

3.2.1. *Effect of BSF and rCF on the fresh properties*

Fig. 11 illustrates how the fresh properties vary with the combined dosages of M−rCFs and BSFs. In particular, the air content of the mixes and the slump flow after strokes (AS) are reported and compared.

The dash-dotted curves highlight the variation of the fresh properties for HP-FRCCs without rCFs, pointing out the effects of the addition of steel fibres only. The addition of steel fibres at up to 2% by volume appears not to entail an adverse effect on the flowability of the composite. There is indeed minimal variation in air content and slump flow, which is consistent with previous research on the subject [64].

The appropriate aspect ratio of the fibres and their smooth surface promote the retention of fresh properties, even at relatively high contents. In particular, the smoothness of the surface is associated with reduced energy loss during flow [65]. It is also recognised that using fine particles facilitates fibre dispersion, which ultimately maintains good flow properties when combined with steel fibres [66]. In addition, each sub-chart examines the impact of incorporating rCFs (up to 1% by volume) at a given BSF dosage. Due to their fineness, rCFs are characterised by a high specific surface area, which significantly alters the workability of the composites, drastically increasing the air content in the fresh state by up to 61%, thereby reducing the slump flow by up to 21%. The

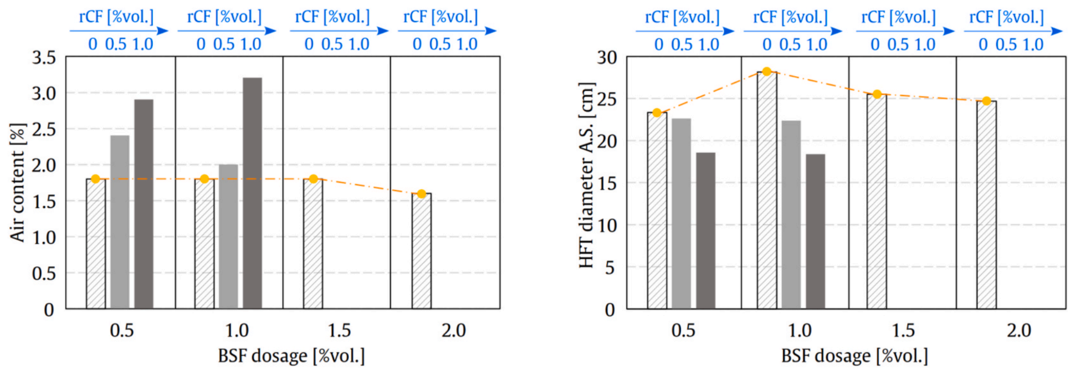

(a) Air content (b) Spread diameter

Fig. 11. LC3-HP-FRCC workability, measured in terms of spread diameter, as a function of the fibre volume fraction. N.B: from here onwards, M−rCF are used.

decreasing trend in the fresh properties of the HP-FRCC under investigation is consistent with other recent studies on CFRC, showcasing a linear relationship with rCF dosage [67]. This makes it clear that a content of rCFs greater than 1% by volume would be unsuitable for most engineering applications, including casting in thin formwork for concrete jacketing, as is being targeted here.

3.2.2. Hardened properties

Fig. 12 compiles the results of the flexural and compressive tests of the investigated hybrid LC^3-based HP-FRCCs (highlighted in yellow), compared to systems including either rCFs or BSFs individually.

The effect of adding 0.5% and 1.0% by volume of M−rCFs to formulations containing 0.5% and 1.0% by volume of BSF is examined, with the aim of selecting suitable composites for jacketing RC columns. In fact, at volumes of BSFs above 1%, even a limited dosage of rCFs may compromise the flowability required for casting the FRC into thin jacketing moulds. The mechanical performance of the hybrid systems relies on a multi-scale synergy between the two fibre types, which target different failure mechanisms [68]. Thanks to their high stiffness and tensile capacity, BSFs become active after cracking, providing macrocrack bridging and governing the flexural (bending) performance. On the other hand, carbon fibres operate at the micro-scale. Due to their fine diameter, they multiply nucleation sites during binder hydration and delay microcrack initiation. As a consequence of hybridisation, the addition of M−rCF increases the bending strength by up to 47% for formulations containing 1% BSF by volume, and by up to 80% for formulations containing 0.5% BSF, thus compensating for the reduced steel fibre content.

In line with the previously observed trend for rCFRC, hybridising BS-FRC with rCFs leads to a steady increase in compressive strength. This more than compensates for the reduced content of virgin BSFs compared to plain BS-FRC, even at 1.5% and 2% vol. Indeed, adding 1% by volume of rCFs to the blend of fibres contributes to an increase in the compressive strength by up to 9%. This improvement is slightly less apparent than that observed for plain rC-HP-FRCCs, due to the role now played by the predominant stiffness of the steel fibres. Fig. 13 reveals the distinct behaviour of the two types of fibre through the optical microscopy analysis of the fracture cross-section of failed specimens. In fact, rCFs fracture extensively within the matrix during the mixing process due to their high aspect ratio and brittle nature, whereas BSFs are gradually pulled out of the embedding matrix. For smooth fibres, the density and quality of the interface zone are the main indicators of the physicochemical bond with the fibres. Previous studies have demonstrated that a dense interfacial transition zone is promoted by low w/b ratios and the extensive use of fine materials in the matrix [69–71], both of which are distinctive characteristics of the current high-performance conglomerate. In this study, the bridging effect is entirely exerted by steel fibres. Their frictional bond during the debonding and extraction phases imparts significant tenacity to the composite, as demonstrated by the results of tensile tests on the selected HP-FRCC formulations. Rather, rCFs appear to be evenly distributed throughout the matrix. Although they do not contribute to crack bridging at the macroscale, their dispersion in the cementitious composite gives them the potential to refine the microstructure effectively. Additionally, their grooved surface improves adhesion to the surrounding matrix and acts as an additional nucleation site for the matrix's early hydration products, locally densifying the C-S-H gel network [72].

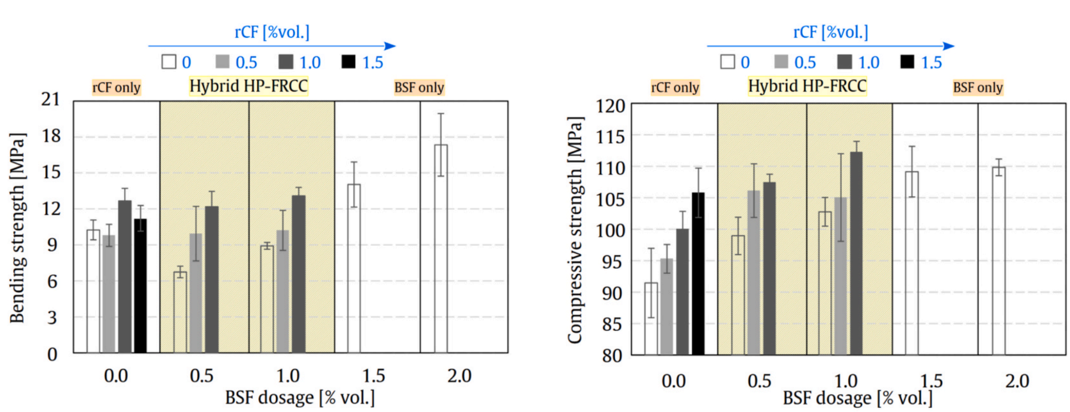

(a) Bending strength (b) Compressive strength

Fig. 12. Trends of HP-FRCC strength as a function of the BSF volume fraction. For BSF volumes below 1.0%, different hybrid compositions with rCFs are considered (shown in grey tones of increasing intensity).

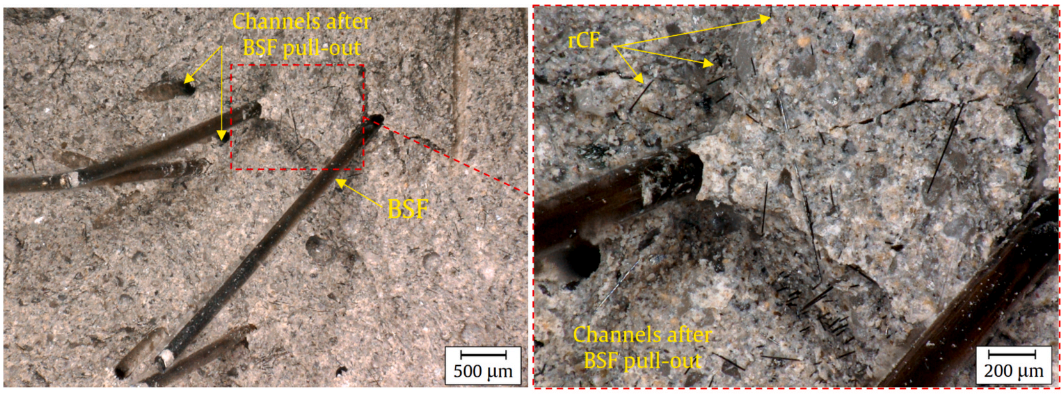

(a) (b)

Fig. 13. Optical microscopy picture of hybrid HP-FRCC. Focus is on the fractured cross-section of a representative sample.

3.3. Pilot application of selected LC^3-HP-FRCC for concrete jacketing

Following the screening campaign presented in Section 3.2, HP-FRCC formulations were selected for the concrete jacketing application based on their combined mechanical performance and fresh-state workability. Regarding the latter, this pilot application requires composite systems with sufficient flowability to be poured into the thin moulds surrounding the columns. To this end, among the mixes presented in the test matrix of Table 3, two formulations incorporating either M−rCFs or BSFs individually (at 1% and 1.5% volume fractions, respectively) were selected as mono-fibre references, against which a hybrid system containing 0.5% M−rCFs and 1% BSFs was assessed. Although the hybrid formulation incorporating 1% M−rCFs and 1% BSFs exhibited the highest mechanical performance during the screening characterisation in Section 3.2.2, its flowability was insufficient for this specific application.

3.3.1. Mechanical characterisation of selected LC^3-HP-FRCC matrices

To provide the material properties required for interpreting the structural response of the confined cylinders, these selected mixtures were mechanically characterised at the same curing age as the jacketing tests. In addition to compression and bending tests, direct tensile tests were performed to evaluate the tensile behaviour, crack development, and energy absorption capacity of the selected HP-FRCCs. Tensile strength was calculated by dividing the maximum tensile load by the cross section of the dog-bone-shaped specimen. The results of the mechanical tests are reported in Table 4 with the Coefficients of Variation (CoV) in brackets. The energy absorption capacity (g) is typically defined as the area under the stress–strain or load–displacement curve, representing the ability of the fibre-reinforced concrete to dissipate energy during the cracking and post-cracking stages [73]. Standardised approaches, such as those proposed by RILEM TC 162-TDF (for tensile tests) and ASTM C1609 (for bending tests), evaluate toughness-related parameters by integrating the response up to a prescribed level of deformation or crack opening. However, as there is no uniquely defined upper limit, the integration range adopted in this study extends up to the point at which the tensile stress decreases to 60% of the peak value, thereby ensuring that the contribution of fibre bridging is consistently captured while excluding the residual tail of the response.

The coefficients of variation (CoV) reported in Table 4 indicate good repeatability of the experimental programme. The compressive and flexural strengths generally exhibit CoV values below 15%, whereas higher variability is observed for tensile strain and energy absorption. This behaviour is typical of HP-FRCCs, as post-cracking parameters are governed by stochastic mechanisms including crack initiation, crack propagation, fibre orientation and local fibre bridging, which naturally introduce greater experimental scatter than strength-related properties. The stress–strain curves obtained from the uniaxial tensile tests, along with the corresponding mean crack width openings, are presented in Fig. 14. Additionally, the strain maps derived from DIC, illustrating the

Table 5
Results of uniaxial compression tests (CoV in round brackets).

Specimen	Peak stress [MPa]	Vertical strain (ε_v) at peak stress* [mm/mm]	Hoop strain (ε_h) at peak stress* [mm/mm]	Strength gain
Ref	10.5 *(3.36%)*	0.00149 *(4.29%)*	0.00635 *(20.93%)*	–
1.0 rCF	14.92 *(8.39%)*	0.00048 *(4.47%)*	0.00409 *(4.50%)*	+ 42%
1.5 BSF	21.77 *(4.52%)*	0.00046 *(4.66%)*	0.00509 *(35.74%)*	+ 107%
1.0 BSF – 0.5 rCF	21.62 *(3.76%)*	0.00078 *(11.86%)*	0.00536 *(10.17%)*	+ 106%

* In the case of the reference specimens the strain is evaluated on the external surface of the unreinforced concrete cylinders.

Table 4
Mechanical properties of HP-FRCC for concrete jacketing after 60 days of curing (CoV in round brackets).

Specimen	Compressive strength σ_c [MPa]	Bending strength σ_f [MPa]	First crack tensile stress $\sigma_{t,crack}$ [MPa]	Tensile strength $\sigma_{t,u}$ [MPa]	Strain at max strength $\varepsilon_{t,u}$ [%]	Energy absorption g [kJ/m^3]
1.0 rFC	102.5 *(2.6%)*	14.9 *(15.5%)*	4.75 *(23.8%)*	4.75 *(23.8%)*	0.027 *(29.5%)*	N.A.* –
1.5 BSF	108.4 *(3.9%)*	17.3 *(12.6%)*	4.92 *(11.9%)*	6.05 *(10.1%)*	0.45 *(35.6%)*	88.60 *(15.42%)*
1.0 BSF – 0.5 rCF	104.7 *(1.6%)*	11.7 *(8.7%)*	5.84 *(11.7%)*	5.84 *(11.7%)*	0.011 *(45.6%)*	19.41 *(7.09%)*

* N.A. = Not applicable. The 1.0 rCF specimens failed immediately after first cracking without a measurable postcracking response; therefore, the energy absorption parameter could not be meaningfully determined.

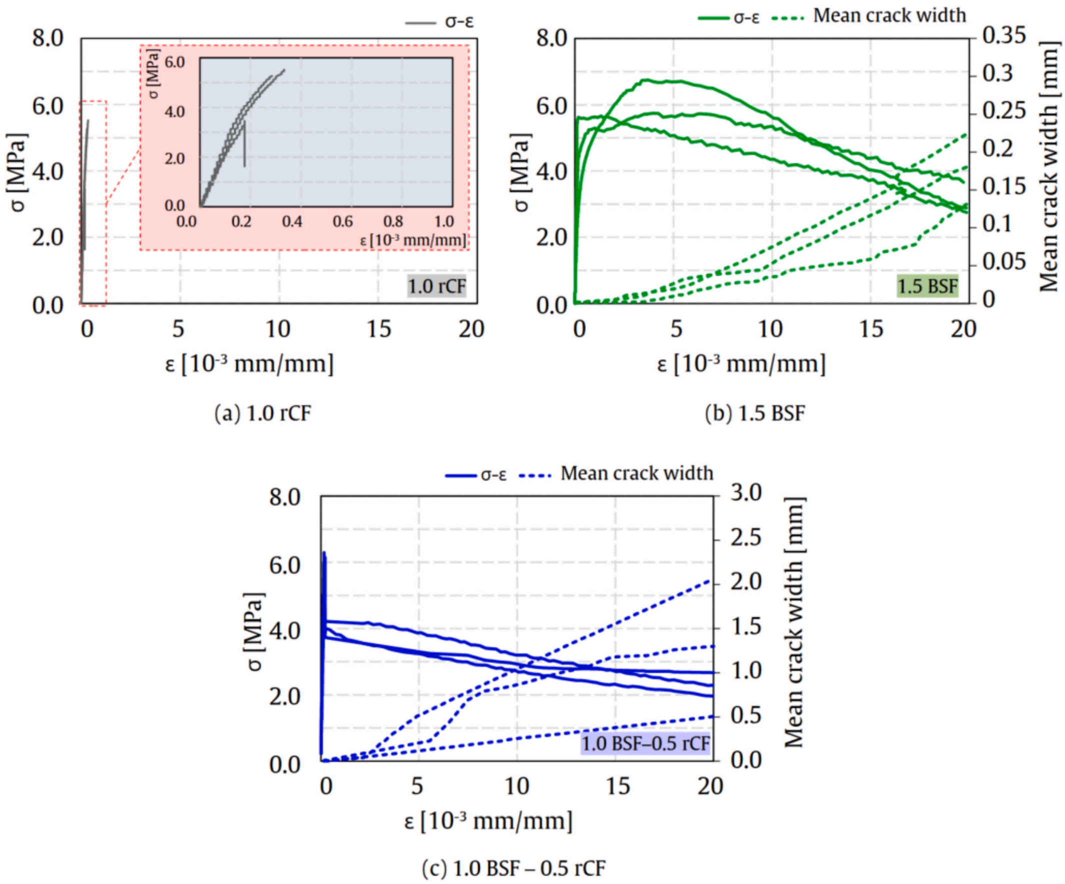

Fig. 14. Tensile stress–strain response of HP-FRCC matrices. For 1.5 BSF and 1.0 BSF-0.5rCF, the variation of the mean crack opening over the tensile test is also plotted (note the different scales).

evolution of matrix cracking during the tensile tests, are shown in Fig. 15.

The results of the compression and bending tests are consistent with those obtained after 28 days of curing, showing a slight increase in mechanical strength after an additional 32 days. The tensile response of the selected HP-FRCC formulations is strongly influenced by the type and dosage of the reinforcing fibres. Specimens containing 1.0% vol. rCFs exhibited linear-elastic behaviour up to the maximum load, followed by brittle tensile failure characterised by the formation of a single crack (Fig. 14a and Fig. 15a). In contrast, the inclusion of BSFs effectively prevented brittle failure. The mix containing 1.5% vol. BSFs developed multiple cracks along the specimen gauge length (see Fig. 15b) and exhibited moderate strain-hardening following first cracking (Fig. 14b). After reaching the maximum load, damage progressively localised at one of the existing cracks, which subsequently propagated, marking the onset of the strain-softening phase.

For the hybrid system (1.0% BSF – 0.5% rCF), the reduced BSF content (1.0% vol.) led to a markedly different response, characterised by strain-softening immediately after the formation of a single crack (see Fig. 14c and Fig. 15c). It is evident that the post-cracking response is governed primarily by the presence and effectiveness of BSFs, which enable fibre bridging and stress transfer across multiple cracks. In contrast, rCFs contribute minimally to post-peak behaviour due to their brittle failure. Nevertheless, their inclusion appears to enhance the first-cracking stress by promoting matrix densification and reducing microstructural defects. This interpretation is supported by the bending test results, which show an increase in first-crack strength with higher rCF content. Moreover, as reported in the literature by Wang et al. [74] and other studies [4,17], the first-cracking stress is only marginally affected by fibre volume fraction and is instead more sensitive to pre-existing flaws in the matrix. Overall, the results reveal a clear hierarchy in energy absorption capacity: the 1.5% BSF mix exhibited the highest toughness, followed by the hybrid system, while the rCF-only mix displayed negligible energy absorption. From a micromechanical perspective, these results confirm that the energy absorption capacity is primarily governed by fibre bridging efficiency and crack distribution. The high toughness observed in the 1.5% BSF mix is associated with stable multiple cracking and sustained stress transfer across cracks, which maximises the area under the stress–strain curve. Conversely, the hybrid system exhibits reduced energy dissipation due to the lower density of bridging fibres and the early localisation of damage, which limits the development of a significant post-peak response.

These findings confirm that BSFs are the primary contributor to toughness enhancement in HP-FRCCs, whereas rCFs play a secondary role, mainly improving the first-crack strength through matrix densification rather than contributing to post-cracking energy dissipation. The crack pattern analysis obtained from DIC further supports these findings. The mix reinforced with 1.5% BSF exhibited relatively uniform crack distribution, with average crack widths ranging between 0.2 and 0.3 mm. In contrast, the hybrid system developed a single dominant crack, with widths reaching up to 2 mm. This behaviour indicates that a BSF content of approximately 1.5% by volume represents a threshold for achieving stable multiple-cracking and strain-hardening behaviour in the investigated matrix, whereas the addition of rCFs primarily enhances crack initiation resistance rather than crack propagation control.

3.3.2. Compression tests on HP-FRCC jacketed concrete cylinders

The strengthening potential of the three selected HP-FRCC matrices was assessed through uniaxial compression tests on laboratory-scale concrete cylinders. Fig. 16 presents the corresponding stress–strain

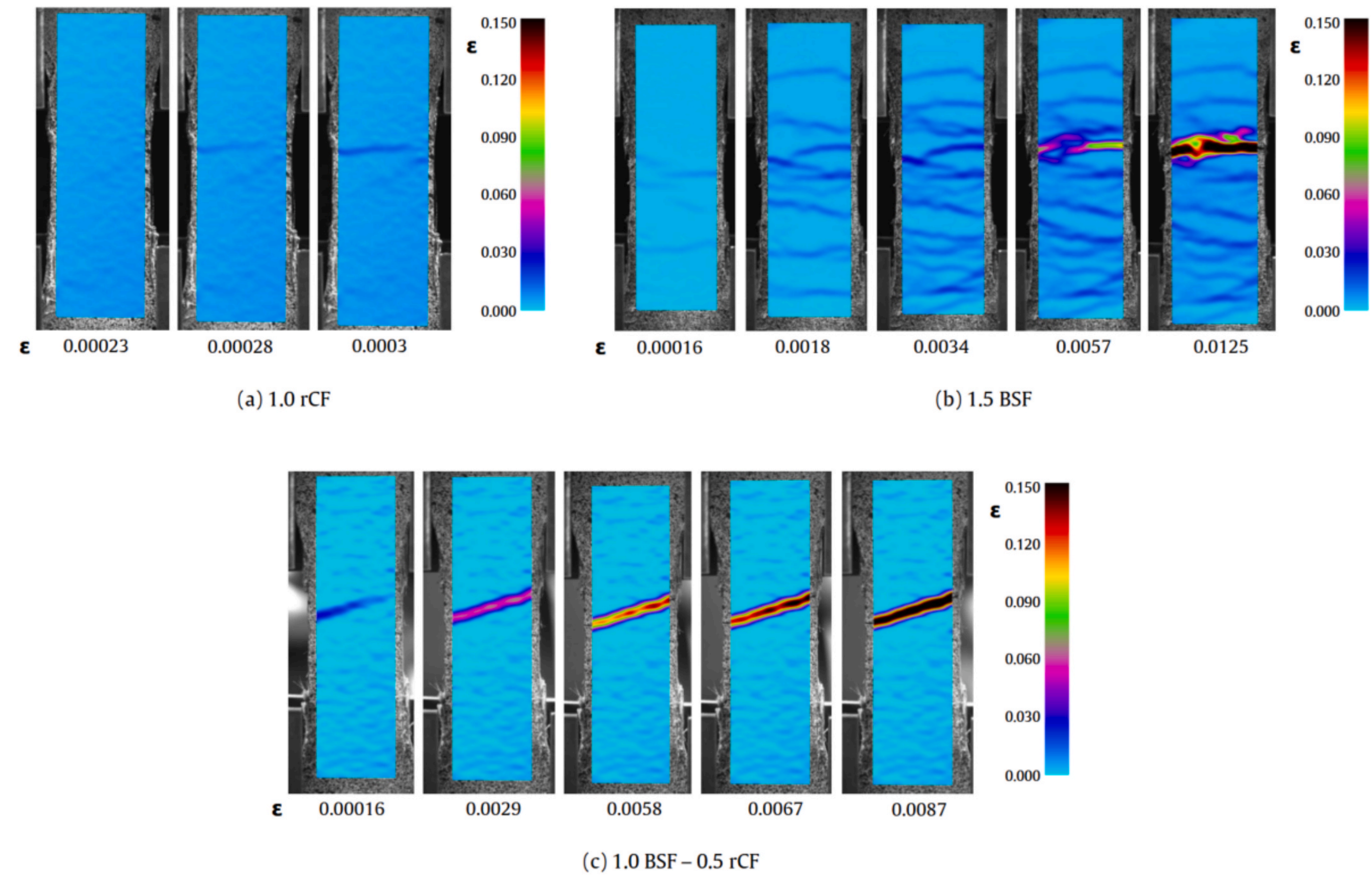

Fig. 15. Frontal strain maps and cracking evolution of dog-bone HP-FRCC specimens under tensile stress.

curves, while full-field strain maps obtained by DIC (Fig. 17) provide detailed insight into the spatial evolution of strains and crack development at five representative stages of loading. Table 5 summarizes the results for each configuration, including peak stress, vertical and hoop strains at peak stress, and strength gain. Unreinforced cylinders failed in a brittle manner, with multiple vertical cracks accompanied by localised spalling and detachment of concrete fragments (Fig. 17a, Fig. 18a and Fig. 19a). All HP-FRCC jackets significantly increased the compressive strength of the concrete cylinders, with peak stresses ranging from 1.42 to 2.07 times that of the unconfined reference. However, the failure mode was strongly influenced by the fibre composition of the jacket.

Cylinders confined with 1.0% rCF HP-FRCC exhibited brittle behaviour, characterised by the formation of two vertical cracks along opposite sides of the jacket, followed by splitting of the internal concrete

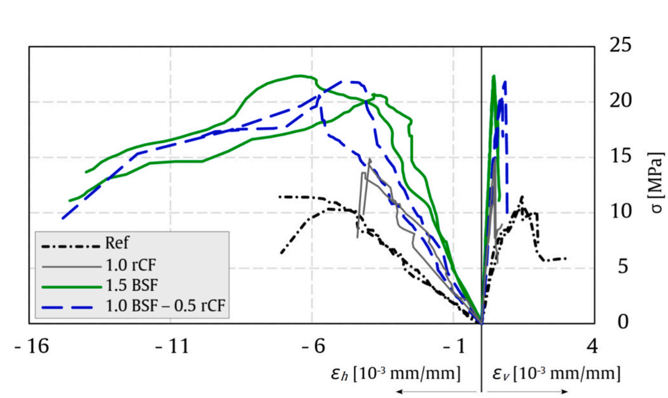

Fig. 16. Stress–strain curves of uniaxial compression tests (evaluated through DIC on the external surface of cylinders).

core (Fig. 18b). In contrast, cylinders reinforced with 1.5% BSF HP-FRCC demonstrated a pseudo-ductile response, achieving approximately a 107% increase in compressive strength and showing distributed cracking rather than sudden localisation. Interestingly, the hybrid system (1.0% BSF – 0.5% rCF) provided a confining effect comparable to that of the 1.5% BSF mix, despite the partial substitution of steel fibres with rCFs. Even at a lower BSF content, the jacket enabled fibre bridging and delayed crack localisation, thereby preventing brittle failure (Fig. 18c and Fig. 18d). The relatively low CoV values obtained for the peak compressive strength confirm the reproducibility of the confinement technique. The larger scatter observed for hoop strain is attributed to the progressive and non-uniform development of cracking in the HP-FRCC jacket, as captured by the DIC measurements, rather than to inconsistencies in the strengthening system itself.

The axial strain (ε_v) of the reinforced specimens was generally lower than that of the unconfined cylinders, which can be attributed to two factors: (i) strain in the reference specimens was measured directly on the concrete surface, whereas in reinforced cylinders it was measured on the stiffer HP-FRCC layer; (ii) the vertical deformation of the jacket depends on stress transfer across the interface, which is limited by the mechanical properties of the inner concrete core. In contrast, the horizontal (hoop) strain (ε_h) response illustrates the benefit of the HP-FRCC jacket: initially, lateral deformation was reduced relative to the unconfined cylinders, but upon matrix cracking and activation of BSF bridging, the reinforced cylinders exhibited significantly higher lateral deformation, reflecting enhanced confinement and ductility.

DIC strain maps revealed distinct damage mechanisms depending on fibre type. rCF-only jackets displayed rapid localisation into two dominant cracks, which propagated progressively with increasing load (Fig. 17b). Conversely, cylinders with BSFs, either alone or in hybrid combination, developed distributed multi-cracking patterns, with

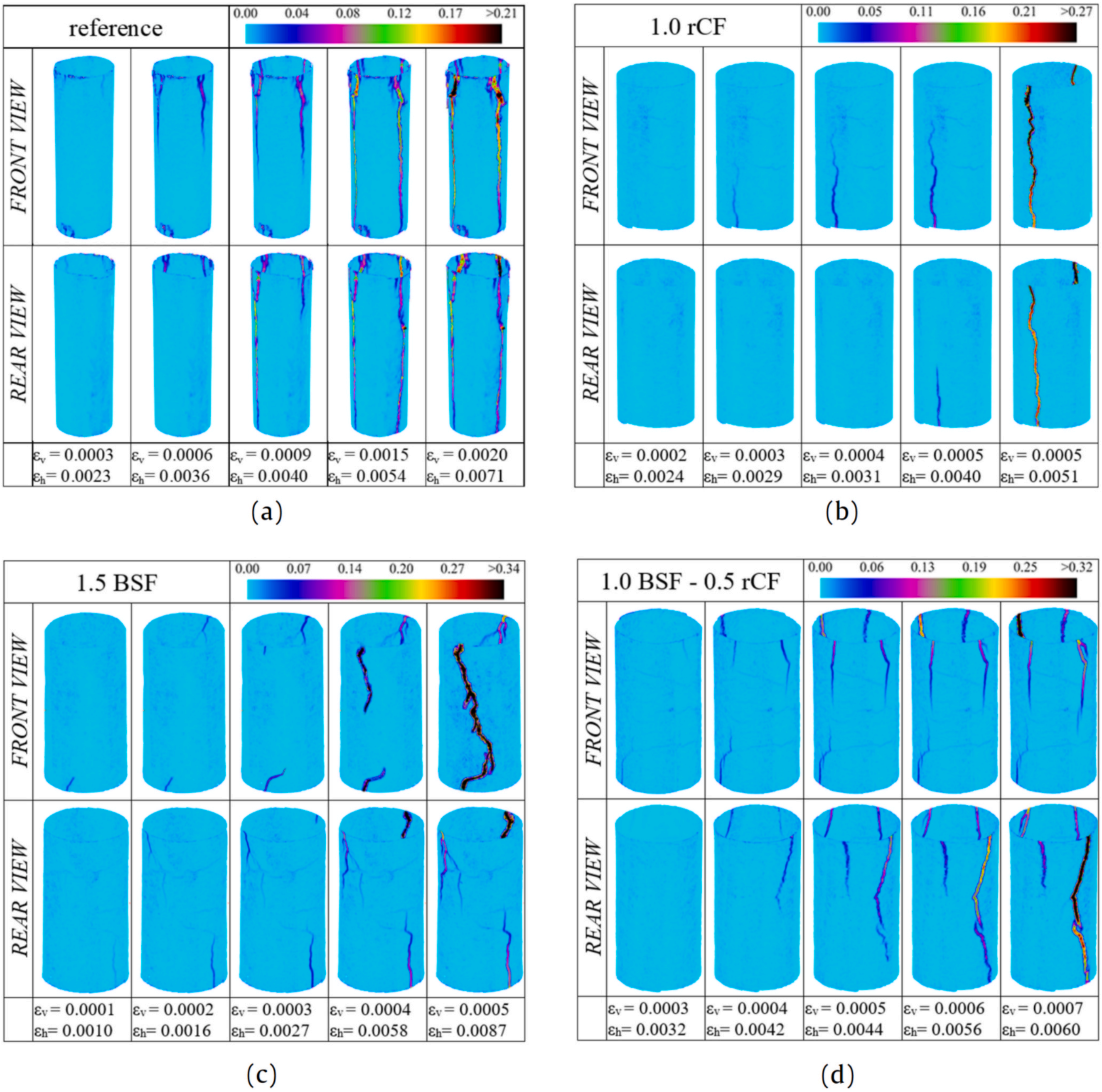

Fig. 17. Strain distribution maps and progression of cracking in (a) reference and (b,c,d) reinforced concrete cylinders during uniaxial compression tests.

multiple independently evolving cracks (Fig. 17c and Fig. 17d). This confirms the essential role of steel fibres in promoting uniform damage distribution, delaying strain localisation, and enhancing post-peak deformation capacity. Closer inspection of the failure modes further supports these findings, as documented in Fig. 18 and Fig. 19. The 1.0% rCF jackets failed in a brittle manner, limiting the confining effect and preventing complete crushing of the internal core (Fig. 19b and Fig. 19b), despite excellent adhesion at the HP-FRCC–concrete interface.

No debonding was observed, indicating reliable bonding between the jacket and substrate. Cylinders reinforced with 1.5% BSF or hybrid jackets, in contrast, exhibited progressive crushing of the core accompanied by distributed surface cracking (Fig. 19c, and Fig. 19d), reflecting effective confinement that remained active beyond peak load. The distributed strain fields in these cases indicate a gradual and controlled damage evolution, in contrast with the abrupt failure of rCF-only jackets.

These results confirm that effective confinement requires not only adequate fibre content but also a fibre type capable of sustaining bridging across multiple cracks. Steel fibres, even at moderate volume fractions, enable pseudo-ductile behaviour and maximize the contribution of the HP-FRCC layer to the overall strength and deformation capacity. The hybrid system benefits from the complementary effect of rCFs in enhancing first-crack stress and matrix densification, while steel fibres maintain post-cracking ductility and energy absorption. From a practical perspective, the hybrid LC^3-HP-FRCC (1.0% BSF–0.5% rCF) achieved confinement performance comparable to that of the 1.5% BSF system while reducing the steel fibre content by approximately 33%. This result demonstrates that recycled carbon fibres can effectively complement steel fibres, reducing the consumption of virgin materials while maintaining structural performance. Combined with the low-clinker LC^3 binder, the proposed hybrid system represents a promising and more sustainable solution for concrete strengthening applications.

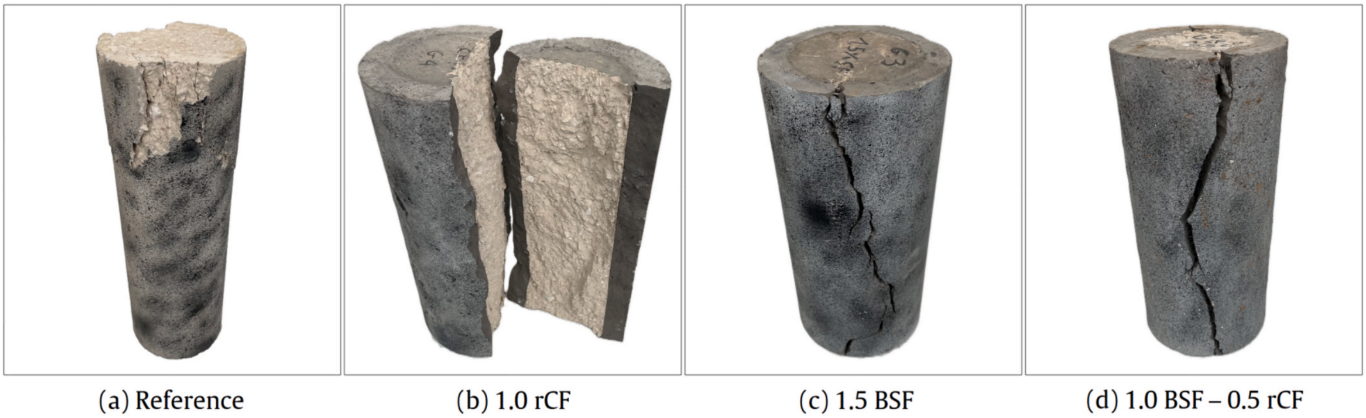

Fig. 18. Failure modes of concrete cylinders after compression tests.

Fig. 19. Upper surface failure of concrete cylinders after compression tests.

3.4. Analytical predictions

In this section the experimental results from the compression tests are compared with analytical predictions derived from recent guidelines and confinement models proposed in the literature. Since no specific design guidelines are yet available for concrete elements reinforced with HP-FRCC, two guidelines originally developed for textile-reinforced mortar (TRM) systems (ACI 549.6R-20 [75] and CNR-DT 215/2018 [76]) were adapted for use in this study. A similar approach was recently adopted by Estevan et al. [39] to evaluate the confinement potential of UHPC in masonry columns.

According to these guidelines, the compressive strength of confined concrete (f_{cc}) is estimated from the unconfined cylinder strength (f_{c0}) as follows:

$$\text{ACI 549}: f_{cc,ACI} = f_{c0} + 3.3 \cdot \psi_f \cdot f_{l,eff} \quad (1)$$

$$\text{CNR DT215}: f_{cc,CNR} = f_{c0} \cdot \left[1 + 2.6 \cdot \left(\frac{f_{l,eff}}{f_{c0}}\right)^{\frac{2}{3}}\right] \quad (2)$$

where $f_{l,eff}$ is the effective lateral confining pressure provided by the external HP-FRCC jacket, ψ_f is a design reduction factor (set equal to 1 in this study). The effective confining pressure is calculated as:

$$f_{l,eff} = k_h \cdot \frac{2\, n_f\, t_f\, E_f\, \varepsilon_{fd}}{D}, \text{ for circular cross sections.} \quad (3)$$

In this study, the above formulation was adapted for confinement using HP-FRCC by substituting the fabric thickness with the jacket thickness ($n_f \bullet t_f = t_{HPFRCC}$), while the term $E_f \bullet \varepsilon_{fd}$ was replaced by the tensile strength of the HP-FRCC ($\sigma_{t,u}$). The horizontal effectiveness coefficient (k_h) was taken as 1 for circular sections, and no limitations were imposed on matrix deformation. Additionally, an analytical formulation proposed by Ronanki et al. [35], based on Mander et al. [77] model, was considered. This model was modified to incorporate the lateral confinement provided by the HP-FRCC jacket instead of traditional reinforcing rebars. The compressive strength of confined concrete cylinders ($f_{cc,Ronanki}$) is expressed as:

$$f_{cc,Ronanki} = f_{c0}\left(-1.254 + 2.254\sqrt{1 + \frac{7.94 f_{l,eff}}{f_{c0}}} - 2\left(\frac{f_{l,eff}}{f_{c0}}\right)\right) \quad (4)$$

The theoretical results provided by equations (1), (2) and (4) were compared to the experimental values ($f_{cc,\exp}/f_{cc,th}$), as reported in Table 6. The analytical models of CNR DT215 and Ronanki et al. closely matched the experimental results for cylinders confined with 1.5% BSF or the hybrid system (1.0 BSF-0.5 rCF). Conversely, for cylinders reinforced solely with 1.0% rCF HP-FRCC, all analytical models overestimated the confined strength. The discrepancy is attributed to the brittle behaviour of rCF matrices, which fail immediately after first cracking and contribute minimally to post-peak stress redistribution.

Table 6
Confined concrete strength (f_{cc}): comparison of experimental results ($f_{cc,\exp}$) with theoretical models and design guidelines ($f_{cc,th}$).

Specimen	$f_{cc,\exp}/f_{c0}$	$f_{cc,\exp}/f_{cc,th}$		
		Ronanki et al.	ACI549 (2020)	CNR DT215 (2018)
1.0 rCF	1.42	0.72	0.88	0.75
1.5 BSF	2.07	0.96	1.16	1.01
1.0 BSF-0.5 rCF	2.06	0.97	1.17	1.02

Pre-existing microstructural flaws may further reduce confinement effectiveness, consistent with the experimental observation of simultaneous failure of the core and rCF jacket (Fig. 18b and Fig. 19b).

These findings emphasise that the effectiveness of existing confinement models strongly depends on the tensile and post-cracking performance of the jacket material. Models calibrated for pseudo-ductile systems or fibre-reinforced matrices tend to over-predict strength when the external layer exhibits brittle post-cracking behaviour or early strain localisation, as in rCF-only HP-FRCC. It should be emphasised that the present validation is limited to laboratory-scale circular concrete cylinders and the three HP-FRCC formulations investigated in this study. Consequently, the proposed adaptation should be regarded as a preliminary validation of the applicability of existing TRM confinement models to HP-FRCC jackets. Further experimental evidence covering different geometries, confinement ratios, jacket thicknesses, concrete strengths and fibre combinations will be required before general design recommendations can be established.

4. Summary and concluding remarks

This study presents the development of hybrid high-performance composites for structural retrofitting, with the aim of promoting circularity and reducing clinker consumption while maintaining high performance target standards. A fine-grained concrete matrix was employed, with a composition tailored to reduce the clinker content by replacing up to 50% of it by mass with limestone and calcined clay.

First, the incorporation of recycled carbon fibres into the LC^3-based matrix was investigated through a comprehensive analysis of their physical and mechanical properties. Next, the effects of a selected type of recycled carbon fibres, combined with commercially available brass-coated steel fibres, on the fresh and hardened properties of the resulting composites were evaluated. Finally, a key application of the selected hybrid carbon-steel fibre-reinforced LC^3 composites as a jacketing layer for laboratory-scale round cylindrical specimens was demonstrated.

The following conclusions can be drawn:

- Despite undergoing similar pyrolysis processes, the two types of recycled carbon fibre derived from different sources and end-of-life FRP materials exhibit markedly different physical and mechanical properties. This highlights the variability of post-consumer sources and the influence of thermal treatment conditions on engineering performance, revealing potential limitations for their widespread use in civil engineering materials. Although sufficient carbon fibre waste from end-of-life FRP exists to meet the demand for high-performance cementitious composites, standardised protocols for retrieval, characterisation, selection, and processing are required to ensure consistent performance.
- Compared to steel fibres, recycled carbon fibres have a pronounced impact on workability and fresh-state properties, limiting their volume fraction to 1% for the intended jacketing application. Careful adjustment of fibre dosage is therefore essential when designing mixtures suitable for different application technologies, such as casting or additive manufacturing.
- While the stiffness and geometry of steel fibres impart significant ductility to hybrid HP-FRCCs, recycled carbon fibres play a key role in strength development. Their fineness and tendency to break during mixing result in an effective filler effect, likely refining the microstructure contributing to increases in compressive and bending strength of up to 20% and 30%, respectively.
- Laboratory-scale concrete cylinders strengthened with HP-FRCC jackets exhibited substantial increases in compressive strength and deformation capacity. The hybrid system (1.0% BSF–0.5% rCF) provided confinement performance comparable to the 1.5% BSF system while reducing the steel fibre content by approximately 33%, demonstrating the potential of recycled carbon fibres to improve the sustainability of strengthening systems without compromising their effectiveness.
- Adapted confinement models, including CNR DT 215 and the model of Ronanki et al., accurately predicted the compressive strength of cylinders confined with BSF or hybrid HP-FRCC jackets. However, these models overestimated the performance of rCF-only jackets due to their brittle post-cracking behaviour and limited contribution to energy absorption. This underscores the need to account for fibre type and post-cracking capacity when applying design models to HP-FRCC-confined concrete.

Overall, the findings confirm that combining steel fibres and recycled carbon fibres in an LC^3-based HP-FRCC matrix enables effective structural retrofitting while promoting material circularity. Steel fibres govern post-cracking toughness and ductility, whereas recycled carbon fibres enhance matrix quality and first-crack resistance. The hybrid system balances these contributions, providing a sustainable and efficient strengthening solution.

Funding and acknowledgment

CS, JD, AJ and ML warmly acknowledge the financial support of the Graduate Academy of the TU Dresden through the exchange programme Lab2Lab for the project "*ARTIST – Advanced Recycled maTerials for Sustainable InfraSTructure*".

The Authors acknowledge RYMYC Srl and Marubeni International (Europe) GmbH for supplying the recycled carbon fibres for this research.

The authors are also grateful to Mr Ameer H. Ahmed, Mr Arun Lila Rai, Ms Annett Willomitzer, and Dr Thomas Köberle for their valuable support in specimen preparation and testing, as well as in conducting TGA and SEM analyses.

CRediT authorship contribution statement

Cesare Signorini: Writing – review & editing, Writing – original draft, Visualization, Validation, Project administration, Methodology, Investigation, Funding acquisition, Formal analysis, Data curation, Conceptualization. **Jacopo Donnini:** Writing – review & editing, Writing – original draft, Visualization, Validation, Methodology, Investigation, Funding acquisition, Formal analysis, Data curation, Conceptualization. **Anna Jose:** Investigation, Data curation. **Gianluca Chiappini:** Investigation, Formal analysis, Data curation. **Marco Liebscher:** Writing – review & editing, Validation, Methodology, Funding acquisition. **Valeria Corinaldesi:** Writing – review & editing, Validation, Methodology, Conceptualization. **Viktor Mechtcherine:** Writing – review & editing, Supervision, Resources.

Declaration of Generative AI and AI-assisted technologies in the writing process

During the preparation of this work the Authors used ChatGPT and Google AI in order to improve the English phrasing and text editing, as well as to generate the visual contents of the Graphical Abstract and flow chart in Fig. 2. After using this tool, the Authors reviewed and edited the content as needed and take full responsibility for the content of the publication.

Declaration of competing interest

The authors declare that they have no known competing financial interests or personal relationships that could have appeared to influence the work reported in this paper.

Data availability

The data sets generated during the current study are available from the corresponding authors on reasonable request.

References

[1] C. Shi, Z. Wu, J. Xiao, D. Wang, Z. Huang, Z. Fang, A review on ultra high performance concrete: part I, Raw Materials and Mixture Design, Construction and Building Materials 101 (2015) 741–751, https://doi.org/10.1016/j.conbuildmat.2015.10.088.

[2] J. Li, Z. Wu, C. Shi, Q. Yuan, Z. Zhang, Durability of ultra-high performance concrete – a review, Constr. Build. Mater. 255 (2020) 119296, https://doi.org/10.1016/j.conbuildmat.2020.119296.

[3] N. Generosi, J. Donnini, V. Corinaldesi, Characterization of Ultra High Performance Fiber Reinforced Concrete (UHPFRC) Tensile Behaviour, in: P. Serna, A. Llano-Torre, J.R. Martí-Vargas, J. Navarro-Gregori (Eds.), Fibre Reinforced Concrete: Improvements and Innovations, Springer International Publishing, Cham, 2021, pp. 1068–1078, 10.1007/978-3-030-58482-5_94.

[4] J. Donnini, G. Lancioni, G. Chiappini, V. Corinaldesi, Uniaxial tensile behavior of ultra-high performance fiber-reinforced concrete (UHPFRC): Experiments and modeling, Compos. Struct. 258 (2021) 113433, https://doi.org/10.1016/j.compstruct.2020.113433.

[5] P. Máca, R. Sovják, P. Konvalinka, Mix design of UHPFRC and its response to projectile impact, Int. J. Impact Eng 63 (2014) 158–163, https://doi.org/10.1016/j.ijimpeng.2013.08.003.

[6] C. Signorini, F. Bracklow, M. Hering, M. Butler, L. Leicht, T. Schubert, M.A. B. Beigh, B. Beckmann, M. Curbach, V. Mechtcherine, Ballistic limit and damage assessment of hybrid fibre-reinforced cementitious thin composite plates under impact loading, Journal of Building Engineering 80 (2023) 108037, https://doi.org/10.1016/j.jobe.2023.108037.

[7] A. Tawfik, C. Signorini, V. Mechtcherine, Direct assessment of the shear behavior of strain-hardening cement-based composites under quasi-static and impact loading: influence of shear span and notch depth, Cem. Concr. Compos. 140 (2023) 105119, https://doi.org/10.1016/j.cemconcomp.2023.105119.

[8] C. Signorini, A. Tawfik, D. Forni, V. Mechtcherine, E. Cadoni, Sensitivity of the test conditions for direct assessment of dynamic shear properties of fibre-reinforced cementitious composites (FRCC) with Split-Hopkinson bar, Cem. Concr. Compos. 163 (2025) 106212, https://doi.org/10.1016/j.cemconcomp.2025.106212.

[9] X. Wang, D. Wu, J. Zhang, R. Yu, D. Hou, Z. Shui, Design of sustainable ultra-high performance concrete: a review, Constr. Build. Mater. 307 (2021) 124643, https://doi.org/10.1016/j.conbuildmat.2021.124643.

[10] M. Farzad, M. Shafieifar, A. Azizinamini, Retrofitting of bridge columns using UHPC, J. Bridge Eng. 24 (2019) 04019121, https://doi.org/10.1061/(ASCE)BE.1943-5592.0001497.

[11] Y. Huang, M.-G. Lee, Y.-C. Kan, W.-C. Wang, Y.-C. Wang, W.-B. Pan, Reinforced concrete beams retrofitted with UHPC or CFRP, Case Stud. Constr. Mater. 17 (2022) e01507, https://doi.org/10.1016/j.cscm.2022.e01507.

[12] R.S. Krishna, S.M.A. Rahman, T. Aziz, F.U.A. Shaikh, Z. Tao, C. Jiang, Optimising LC3 composites with alternative calcined clays: hydration, strength, and CO_2 reduction, Sustain. Mater. Technol. 48 (2026) e02042, https://doi.org/10.1016/j.susmat.2026.e02042.

[13] R. Snellings, G. Mertens, J. Elsen, Supplementary Cementitious Materials, Rev. Mineral. Geochem. 74 (2012) 211–278, https://doi.org/10.2138/rmg.2012.74.6.

[14] K. Scrivener, F. Martirena, S. Bishnoi, S. Maity, Calcined clay limestone cements (LC3), Cem. Concr. Res. 114 (2018) 49–56, https://doi.org/10.1016/j.cemconres.2017.08.017.

[15] K.L. Scrivener, V.M. John, E.M. Gartner, Eco-efficient cements: potential economically viable solutions for a low-CO2 cement-based materials industry, Cem. Concr. Res. 114 (2018) 2–26, https://doi.org/10.1016/j.cemconres.2018.03.015.

[16] L. Wang, N. Ur Rehman, I. Curosu, Z. Zhu, M.A.B. Beigh, M. Liebscher, L. Chen, D. C.W. Tsang, S. Hempel, V. Mechtcherine, On the use of limestone calcined clay cement (LC3) in high-strength strain-hardening cement-based composites (HS-SHCC), Cement and Concrete Research 144 (2021) 106421, https://doi.org/10.1016/j.cemconres.2021.106421.

[17] A.H. Ahmed, C. Signorini, M. Chikhradze, M. Liebscher, M. Butler, V. Mechtcherine, Employing limestone and calcined clay for preserving the strain-hardening response of PET fiber-reinforced cementitious composites, Constr. Build. Mater. 438 (2024) 137166, https://doi.org/10.1016/j.conbuildmat.2024.137166.

[18] A.H. Ahmed, S. Nune, M. Liebscher, T. Köberle, A. Willomitzer, I. Noack, M. Butler, V. Mechtcherine, Exploring the role of dilutive effects on microstructural development and hydration kinetics of limestone calcined clay cement (LC3) made of low-grade raw materials, J. Clean. Prod. 428 (2023) 139438, https://doi.org/10.1016/j.jclepro.2023.139438.

[19] H. Abdolpour, P. Niewiadomski, Ł. Sadowski, Recycling of steel fibres and spent equilibrium catalyst in ultra-high performance concrete: Literature review, research gaps, and future development, Constr. Build. Mater. 309 (2021) 125147, https://doi.org/10.1016/j.conbuildmat.2021.125147.

[20] M.H. Abd-Elrahman, I.S. Agwa, Y. Elsakhawy, M.S. Rizk, Effect of utilising ferrosilicon and recycled steel fibres on ultra-high-strength concrete containing recycled granite, Case Stud. Constr. Mater. 18 (2023) e01903, https://doi.org/10.1016/j.cscm.2023.e01903.

[21] R. Merli, M. Preziosi, A. Acampora, M.C. Lucchetti, E. Petrucci, Recycled fibers in reinforced concrete: a systematic literature review, J. Clean. Prod. 248 (2020) 119207, https://doi.org/10.1016/j.jclepro.2019.119207.

[22] A. Patchen, S. Young, D. Penumadu, An investigation of mechanical properties of recycled carbon fiber reinforced ultra-high-performance concrete, Materials 16 (2022) 314, https://doi.org/10.3390/ma16010314.

[23] S. Tiwari, J. Bijwe, Surface treatment of carbon fibers - a review, Procedia Technol. 14 (2014) 505–512, https://doi.org/10.1016/j.protcy.2014.08.064.

[24] J. Donnini, G. Lancioni, V. Corinaldesi, Failure modes in FRCM systems with dry and pre-impregnated carbon yarns: Experiments and modeling, Compos. B Eng. 140 (2018) 57–67, https://doi.org/10.1016/j.compositesb.2017.12.024.

[25] A. Alatawna, R. Sripada, L. Nahum, M. Birenboimi, O. Regev, A. Peled, Textile-cement bond enhancement: Sprinkle some hydrophilic powder, Cem. Concr. Compos. 120 (2021) 104031, https://doi.org/10.1016/j.cemconcomp.2021.104031.

[26] S. Karuppannan Gopalraj, T. Kärki, A review on the recycling of waste carbon fibre/glass fibre-reinforced composites: fibre recovery, properties and life-cycle analysis, SN, Appl. Sci. 2 (2020) 433, https://doi.org/10.1007/s42452-020-2195-4.

[27] M.A. Nahil, P.T. Williams, Recycling of carbon fibre reinforced polymeric waste for the production of activated carbon fibres, J. Anal. Appl. Pyrol. 91 (2011) 67–75, https://doi.org/10.1016/j.jaap.2011.01.005.

[28] J.A. Butenegro, M. Bahrami, J. Abenojar, M.Á. Martínez, Recent progress in carbon fiber reinforced polymers recycling: a review of recycling methods and reuse of carbon fibers, Materials 14 (2021) 6401, https://doi.org/10.3390/ma14216401.

[29] A. Meda, S. Mostosi, P. Riva, Shear strengthening of reinforced concrete beam with high-performance fiber-reinforced cementitious composite jacketing, SJ 111 (2014) 1059–1068. https://doi.org/10.14359/51687027.

[30] J. Donnini, S. Spagnuolo, V. Corinaldesi, A comparison between the use of FRP, FRCM and HPM for concrete confinement, Compos. B Eng. 160 (2019) 586–594, https://doi.org/10.1016/j.compositesb.2018.12.111.

[31] A. Reggia, A. Morbi, G.A. Plizzari, Experimental study of a reinforced concrete bridge pier strengthened with HPFRC jacketing, Eng. Struct. 210 (2020) 110355, https://doi.org/10.1016/j.engstruct.2020.110355.

[32] P. Cassese, C. Menna, A. Occhiuzzi, D. Asprone, Experimental behavior of existing RC columns strengthened with HPFRC jacket under concentric and eccentric compressive load, Buildings 11 (2021) 521, https://doi.org/10.3390/buildings11110521.

[33] S. Ali Dadvar, D. Mostofinejad, H. Bahmani, Strengthening of RC columns by ultra-high performance fiber reinforced concrete (UHPFRC) jacketing, Construction and Building Materials 235 (2020) 117485, https://doi.org/10.1016/j.conbuildmat.2019.117485.

[34] M. Del Zoppo, C. Menna, M. Di Ludovico, D. Asprone, A. Prota, Opportunities of light jacketing with Fibre Reinforced Cementitious Composites for seismic retrofitting of existing RC columns, Compos. Struct. 263 (2021) 113717, https://doi.org/10.1016/j.compstruct.2021.113717.

[35] V.S. Ronanki, S. Aaleti, Experimental and analytical investigation of UHPC confined concrete behavior, Constr. Build. Mater. 325 (2022) 126710, https://doi.org/10.1016/j.conbuildmat.2022.126710.

[36] B. Lopes Poncetti, V. Brother Dos Santos, C. Coelho De Magalhães Grossi, L. Dezotti Tolentino, R., Dias Vanderlei, Experimental investigation of the performance of normal and high-strength concrete confined by UHPFRC jacketing, Engineering Structures 289 (2023) 116321, https://doi.org/10.1016/j.engstruct.2023.116321.

[37] J. Xie, Q. Fu, J.-B. Yan, Compressive behaviour of stub concrete column strengthened with ultra-high performance concrete jacket, Constr. Build. Mater. 204 (2019) 643–658, https://doi.org/10.1016/j.conbuildmat.2019.01.220.

[38] B. Peng, S. Wei, L. Long, Q. Zheng, Y. Ma, L. Chen, Experimental Investigation on the Performance of Historical Squat Masonry Walls Strengthened by UHPC and Reinforced Polymer Mortar Layers, Appl. Sci. 9 (2019) 2096, https://doi.org/10.3390/app9102096.

[39] L. Estevan, B. Torres, F.J. Baeza, V. Gattulli, S. Ivorra, Enhancing fire resistance of masonry structures: the potential of ultra high performance concrete (UHPC), Constr. Build. Mater. 425 (2024) 136088, https://doi.org/10.1016/j.conbuildmat.2024.136088.

[40] A. Baziak, K. Pławecka, I. Hager, A. Castel, K. Korniejenko, Development and Characterization of Lightweight Geopolymer Composite Reinforced with Hybrid Carbon and Steel Fibers, Materials 14 (2021) 5741, https://doi.org/10.3390/ma14195741.

[41] C. Hu, C. Signorini, V. Mechtcherine, Effectiveness of Sprayed Strain-Hardening Limestone Calcined Clay Cement (SHLC3) Composites in Retrofitting Concrete-Beams, in: V. Mechtcherine, C. Signorini, D. Junger (Eds.), Transforming Construction: Advances in Fiber Reinforced Concrete, Springer Nature Switzerland, Cham, 2024: pp. 810–818. https://doi.org/10.1007/978-3-031-70145-0_96.

[42] M.A.B. Beigh, C. Signorini, A. Rauf, C. Schröfl, T. Köberle, K. Grahl, T. Matschei, V. Mechtcherine, Intrinsic rheological behavior of limestone calcined clay cementitious (LC3) binders for automated construction: effect of calcium sulfate varieties, Constr. Build. Mater. 477 (2025) 141314, https://doi.org/10.1016/j.conbuildmat.2025.141314.

[43] C. Hu, S. Reißig, V. Mechtcherine, Influence of air pressure on the rheological behaviour of shotcrete fibre-reinforced cementitious composites for structural strengthening, MATEC Web Conf. 409 (2025) 11004, https://doi.org/10.1051/matecconf/202540911004.

[44] A.H. Ahmed, J. Hübner, D. Junger, C. Signorini, M. Butler, M. Liebscher, C. Scheffler, V. Mechtcherine, Engineering low clinker Strain-Hardening cementitious composites (SHCC) using polyethylene and cost-effective

polypropylene fibers: an experimental scale-linking analysis, Mater. Des. 254 (2025) 114051, https://doi.org/10.1016/j.matdes.2025.114051.
[45] M. Ranjbarian, V. Mechtcherine, A novel test setup for the characterization of bridging behaviour of single microfibres embedded in a mineral-based matrix, Cem. Concr. Compos. 92 (2018) 92–101, https://doi.org/10.1016/j.cemconcomp.2018.05.017.
[46] H. Li, M. Liebscher, K.H. Ly, P.V. Ly, T. Köberle, J. Yang, Q. Fan, M. Yu, I. M. Weidinger, V. Mechtcherine, Effect of electrophoretic deposition of micro-quartz on the microstructural and mechanical properties of carbon fibers and their bond performance toward cement, J. Mater. Sci. 57 (2022) 21885–21900, https://doi.org/10.1007/s10853-022-07989-w.
[47] H. Li, J. Yang, L. Wang, L. Li, Y. Xia, T. Köberle, W. Dong, N. Zhang, B. Yang, V. Mechtcherine, Multiscale assessment of performance of limestone calcined clay cement (LC3) reinforced with virgin and recycled carbon fibers, Constr. Build. Mater. 406 (2023) 133228, https://doi.org/10.1016/j.conbuildmat.2023.133228.
[48] A. Belli, A. Mobili, T. Bellezze, P.B. Cachim, F. Tittarelli, Self-Sensing Mortars with Recycled Carbon-based Fillers and Fibers. SP-355: Recent Advances in Concrete Technology and Sustainability Issues, American Concrete Institute, 2022.
[49] W. Guo, S. Bai, Y. Ye, L. Zhu, Recycling carbon fiber-reinforced polymers by pyrolysis and reused to prepare short-cut fiber C/C composite, J. Reinf. Plast. Compos. 38 (2019) 340–348, https://doi.org/10.1177/0731684418822144.
[50] J. Meredith, S. Cozien-Cazuc, E. Collings, S. Carter, S. Alsop, J. Lever, S.R. Coles, B. M. Wood, K. Kirwan, Recycled carbon fibre for high performance energy absorption, Compos. Sci. Technol. 72 (2012) 688–695, https://doi.org/10.1016/j.compscitech.2012.01.017.
[51] S.M.C. Alves, F.S. Da Silva, M.V. Donadon, R.R. Garcia, E.J. Corat, Process and characterization of reclaimed carbon fiber composites by pyrolysis and oxidation, assisted by thermal plasma to avoid pollutants emissions, J. Compos. Mater. 52 (2018) 1379–1398, https://doi.org/10.1177/0021998317724214.
[52] G. Jiang, S.J. Pickering, Structure–property relationship of recycled carbon fibres revealed by pyrolysis recycling process, J. Mater. Sci. 51 (2016) 1949–1958, https://doi.org/10.1007/s10853-015-9502-2.
[53] A. Yasmin, I.M. Daniel, Mechanical and thermal properties of graphite platelet/epoxy composites, Polymer 45 (2004) 8211–8219, https://doi.org/10.1016/j.polymer.2004.09.054.
[54] F. Yang, G. Hu, H. He, M. Yi, Y. Ge, L. Ran, K. Peng, Effect of amorphous carbon on the tensile behavior of polyacrylonitrile (PAN)-based carbon fibers, J. Mater. Sci. 54 (2019) 8800–8813, https://doi.org/10.1007/s10853-018-03256-z.
[55] E. Mansfield, A. Kar, S.A. Hooker, Applications of TGA in quality control of SWCNTs, Anal. Bioanal. Chem. 396 (2010) 1071–1077, https://doi.org/10.1007/s00216-009-3319-2.
[56] J. Donnini, C. Signorini, V. Corinaldesi, V. Mechtcherine, Use of Recycled and Virgin Carbon Fibers in Limestone Calcined Clay Cement Composites, in: V. Mechtcherine, C. Signorini, D. Junger (Eds.), Transforming Construction: Advances in Fiber Reinforced Concrete, Springer Nature Switzerland, Cham, 2024: pp. 75–82. https://doi.org/10.1007/978-3-031-70145-0_10.
[57] M. Monazami, R. Gupta, Investigation of mechanical behavior and fracture energy of fiber-reinforced concrete beams and panels, Cem. Concr. Compos. 133 (2022) 104656, https://doi.org/10.1016/j.cemconcomp.2022.104656.
[58] M. Li, H. Wang, C. Zhang, S. Deng, K. Li, X. Guo, The effect of graphene oxide grafted carbon fiber on mechanical properties of class G Portland cement, J. Adhes. Sci. Technol. 33 (2019) 2494–2516, https://doi.org/10.1080/01694243.2019.1646848.
[59] W. Meng, K.H. Khayat, Mechanical properties of ultra-high-performance concrete enhanced with graphite nanoplatelets and carbon nanofibers, Compos. B Eng. 107 (2016) 113–122, https://doi.org/10.1016/j.compositesb.2016.09.069.
[60] B. Han, L. Zhang, C. Zhang, Y. Wang, X. Yu, J. Ou, Reinforcement effect and mechanism of carbon fibers to mechanical and electrically conductive properties of cement-based materials, Constr. Build. Mater. 125 (2016) 479–489, https://doi.org/10.1016/j.conbuildmat.2016.08.063.
[61] N. Banthia, S.M. Soleimani, Flexural Response of Hybrid Fiber-Reinforced Cementitious Composites, ACI Mater. J. 102 (2005) 382–389. https://doi.org/10.14359/14800.
[62] M. Kimm, A. Sabir, T. Gries, P. Suwanpinij, Potential of using Recycled Carbon Fibers as reinforcing Material for Fiber Concrete, in: P. Serna, A. Llano-Torre, J. R. Martí-Vargas, J. Navarro-Gregori (Eds.), Fibre Reinforced Concrete: Improvements and Innovations, Springer International Publishing, Cham, 2021, pp. 949–960, https://doi.org/10.1007/978-3-030-58482-5_83.
[63] W. Song, J. Yin, Hybrid effect Evaluation of Steel Fiber and Carbon Fiber on the Performance of the Fiber Reinforced Concrete, Materials 9 (2016) 704, https://doi.org/10.3390/ma9080704.
[64] O. Gencel, W. Brostow, T. Datashvili, M. Thedford, Workability and Mechanical Performance of Steel Fiber-Reinforced Self-Compacting Concrete with Fly Ash, Compos. Interfaces 18 (2011) 169–184, https://doi.org/10.1163/092764411X567567.
[65] M. Sahmaran, A. Yurtseven, I., Ozgur Yaman, Workability of hybrid fiber reinforced self-compacting concrete, Build. Environ. 40 (2005) 1672–1677, https://doi.org/10.1016/j.buildenv.2004.12.014.
[66] W. Wang, A. Shen, Z. Lyu, Z. He, K.T.Q. Nguyen, Fresh and rheological characteristics of fiber reinforced concrete——A review, Constr. Build. Mater. 296 (2021) 123734, https://doi.org/10.1016/j.conbuildmat.2021.123734.
[67] Md. Safiuddin, G. Abdel-Sayed, N. Hearn, Effects of Pitch-based Short Carbon Fibers on the Workability, Unit Weight, and Air Content of Mortar Composite, Fibers 6 (2018) 63, https://doi.org/10.3390/fib6030063.
[68] M. Khan, M. Cao, M. Ali, Cracking behaviour and constitutive modelling of hybrid fibre reinforced concrete, Journal of Building Engineering (2020) 101272, https://doi.org/10.1016/j.jobe.2020.101272.
[69] Z. Wu, C. Shi, K.H. Khayat, S. Wan, Effects of different nanomaterials on hardening and performance of ultra-high strength concrete (UHSC), Cem. Concr. Compos. 70 (2016) 24–34, https://doi.org/10.1016/j.cemconcomp.2016.03.003.
[70] Z. Wu, K.H. Khayat, C. Shi, Effect of nano-SiO2 particles and curing time on development of fiber-matrix bond properties and microstructure of ultra-high strength concrete, Cem. Concr. Res. 95 (2017) 247–256, https://doi.org/10.1016/j.cemconres.2017.02.031.
[71] Y. Deng, Z. Zhang, C. Shi, Z. Wu, C. Zhang, Steel Fiber–Matrix Interfacial Bond in Ultra-High Performance Concrete: a Review, Engineering 22 (2023) 215–232, https://doi.org/10.1016/j.eng.2021.11.019.
[72] A. Akbar, V.K.R. Kodur, K.M. Liew, Microstructural changes and mechanical performance of cement composites reinforced with recycled carbon fibers, Cem. Concr. Compos. 121 (2021) 104069, https://doi.org/10.1016/j.cemconcomp.2021.104069.
[73] M. Xu, K. Wille, Fracture energy of UHP-FRC under direct tensile loading applied at low strain rates, Compos. B Eng. 80 (2015) 116–125, https://doi.org/10.1016/j.compositesb.2015.05.031.
[74] Y. Wang, P. Qiao, J. Sun, A. Chen, Influence of fibers on tensile behavior of ultra-high performance concrete: a review, Constr. Build. Mater. 430 (2024) 136432, https://doi.org/10.1016/j.conbuildmat.2024.136432.
[75] Aci, PRC-549.4-20, Guide to Design and Construction of Externally Bonded Fabric-Reinforced and Steel-Reinforced Grout Systems for Repair and Strengthening of Concrete Structures, American Concrete Institute (2020).
[76] CNR DT215, Guide for the Design and Construction of Externally Bonded Fibre Reinforced Inorganic Matrix Systems for Strengthening Existing Structures, 2018.
[77] J.B. Mander, M.J.N. Priestley, R. Park, Theoretical Stress-Strain Model for Confined Concrete, J. Struct. Eng. 114 (1988) 1804–1826, https://doi.org/10.1061/(ASCE)0733-9445(1988)114:8(1804).